2	RNA-binding proteins contribute to small RNA loading in plant extracellular
3	vesicles
4	Baoye He ^{1,4} , Qiang Cai ^{1,2,4} , Lulu Qiao ¹ , Chien-Yu Huang ¹ , Shumei Wang ¹ , Weili
5	Miao ³ , Tommy Ha ¹ , Yinsheng Wang ³ and Hailing Jin ^{1*}
6 7 8	¹ Department of Microbiology and Plant Pathology, Center for Plant Cell Biology, Institute for Integrative Genome Biology, University of California, Riverside, CA, USA
9 10	² State Key Laboratory of Hybrid Rice, College of Life Science, Wuhan University, Wuhan, China
11 12	³ Department of Chemistry, Center for Plant Cell Biology, Institute for Integrative Genome Biology, University of California, Riverside, CA, USA
13	
14	⁴ These authors contributed equally
15	
16	*Correspondence: hailingj@ucr.edu
17	
18	
19	

Abstract

Plants use extracellular vesicles (EVs) to transport small RNAs (sRNAs) into their fungal pathogens and silence fungal virulence-related genes through a phenomenon called 'cross-kingdom RNAi'. It remains unknown, however, how sRNAs are selectively loaded into EVs. Here, we identified several RNA-binding proteins in *Arabidopsis*, including Argonaute 1 (AGO1), RNA helicases (RHs) and annexins (ANNs), which are secreted by exosome-like EVs. AGO1, RH11 and RH37 selectively bind to EV-enriched sRNAs but not to non-EV associated sRNAs, suggesting that they contribute to the selective loading of sRNAs into EVs. Conversely, ANN1 and ANN2 bind to sRNAs non-specifically. The *ago1*, *rh11rh37* and *ann1ann2* mutants showed reduced secretion of sRNAs in EVs, demonstrating that these RNA-binding proteins play an important role in sRNA loading and/or stabilization in EVs. Furthermore, *rh11rh37* and *ann1ann2* showed increased susceptibility to *Botrytis cinerea*, suggesting that RH11, RH37, ANN1 and ANN2 positively regulate plant immunity against *B. cinerea*.

Editor's Summary

Plants use extracellular vesicles to deliver small RNAs that could silence fungal virulence genes to their fungal pathogens. In this study, the authors profile the components of these extracellular vesicles and investigate regulators contributing to the specific RNA loading and stabilization.

Main

41

42

43

44

45

46

47

48

49

50

51

52

53

54

55

56

57

58

59

60

61

62

Small RNAs (sRNAs) induce RNA interference (RNAi) and play an important role in regulating host immune responses and pathogen virulence 1, 2, 3. In addition to their role in regulating gene expression endogenously, sRNAs can travel between interacting organisms to induce gene silencing in the counterparty in trans, a phenomenon called 'cross-kingdom RNAi' 4-7. We discovered that fungal pathogens can deliver sRNAs into host plants and hijack host RNAi machinery to silence plant immunity genes⁵. Further, we demonstrated that cross-kingdom RNAi is bidirectional 4, 8, host plants can use extracellular vesicles (EVs) to transport sRNAs into interacting fungal cells to suppress the expression of fungal virulence-related genes ⁴. EVs are secreted membrane-encased vesicular compartments that play important roles in communication between cells and interacting organisms by transporting proteins, lipids, RNAs and other molecules 9. EVs released by mammalian cells can be divided into three major categories on the basis of their distinct biogenesis pathways and specific protein markers, including exosomes, microvesicles and apoptotic bodies ¹⁰. Exosomes are small vesicles derived from multivesicular bodies (MVBs) and are released as a consequence of the fusion of the outer membrane of MVBs with the plasma membrane ⁹. Microvesicles are formed and released by direct budding from the plasma membrane and apoptotic bodies are formed during the execution phase of the apoptotic process ¹⁰. In mammalian systems, multiple classes of EVs, especially exosomes, have been shown to transport RNAs into specific recipient cells within an organism ¹¹⁻¹⁴. Recently, we discovered that *Arabidopsis* cells secrete exosome-like

EVs to deliver sRNAs into fungal pathogen Botrytis cinerea 4, providing the first example of a host sRNA delivery mechanism in any interacting system. These sRNAcontaining EVs are enriched in tetraspanin TET8 and TET9 proteins which are the orthologues of mammalian exosome markers — tetraspanins CD63, CD81, and CD9 15. Meanwhile, TET8 colocalizes with MVB markers inside the cells, indicating that TET8-positive EVs are plant exosome-like EVs. These studies have expanded the known function of EVs to include cross-kingdom trafficking of functional sRNAs. We found that the expression profile of EV-enriched sRNAs is distinct from that of total sRNAs isolated from the same tissue ⁴. Reports from mammalian systems also determined that EVs had RNA expression profiles distinct from total cellular RNAs. ¹⁶-¹⁸. These studies suggest that sorting of RNAs into EV is a precisely regulated process. However, how sRNAs are selectively loaded and stabilized in exosomes is largely unknown. In this study, we identified a group of RNA binding proteins (RBPs) in plant EVs, mainly TET-positive exosome-like vesicles, including argonaute protein 1 (AGO1), DEAD-box RNA helicases (RHs) and annexins (ANNs). AGO proteins complex with sRNAs to induce the silencing of genes with complementary sequences¹. The Arabidopsis genome encodes ten AGOs with selective sRNA binding activities ¹⁹. AGO1 preferentially binds to 20-22 nucleotide sRNAs with a 5'-terminal uridine, whereas AGO2 and AGO4 favor sRNAs with a 5'-terminal adenosine and AGO5 predominantly binds sRNAs beginning with a cytosine²⁰. Furthermore, the secondary structure of an sRNA duplex can also affect its loading efficiency into AGO proteins²¹.

63

64

65

66

67

68

69

70

71

72

73

74

75

76

77

78

79

80

81

82

83

DEAD-box RHs contain a conserved Asp-Glu-Ala-Asp (DEAD) motif. They bind and rearrange the secondary structure of RNAs in an energy-dependent manner ^{22,23}. Here, we show that EV-associated AGO1, RH11 and RH37 specifically bind to EV-enriched sRNAs and co-localize with MVBs in the cell, which facilitates the packaging of these RBPs and their associated sRNAs into MVB-derived EVs. The ANNs, however, bind to sRNAs non-specifically and may only contribute to the stabilization of EV-encased sRNAs. Moreover, the *rh11rh37* and *ann1ann2* mutants were more susceptible to *B. cinerea* than wild-type plants and the fungal target genes of transferred plant sRNAs were derepressed in *B. cinerea* purified from infected *rh11rh37* and *ann1ann2*. These findings further support that EV-localized RBPs contribute to sorting and stabilizing plant secreted sRNAs in EVs.

Results

Proteomic analysis reveals a group of RBPs in plant EVs

We hypothesize that a set of EV-associated proteins, specifically RBPs, may be responsible for the selective loading of sRNAs into EVs. To identify EV-associated proteins, we isolated EVs from the apoplastic fluid of *Arabidopsis* rosette leaves and performed proteomic analysis using mass spectrometry (MS) (Extended Data Fig. 1) ⁴. Specifically, we used *B. cinerea*-infected leaves, and centrifuged at 100,000g (P100) to increase the yield of isolated TET8-positive EVs because we previously showed that fungal infection increases EV secretion (Extended Data Fig. 1)⁴. Proteins detected in all three biological replicates with distinct peptide counts of five or more in each

replicate were further analysed for gene ontology (GO) terms related to biological process and molecular function (Supplementary Table 1 and Extended Data Fig. 2). Among the identified proteins, 28.24% were categorized by GO terms as stress response proteins and 14.88% were categorized as response to biotic stimulus proteins, both of which were enriched in EV fractions, suggesting that EVs are involved in defense response and stress adaption processes. A total of 93 RBPs were detected with at least five distinct peptides in each of the three biological replicates (Supplementary Table 2). We selected the RBPs that have potential sRNA-binding activity for further analysis, including AGO1 (nine peptides), DEAD-box RNA helicases RH11 (11 peptides), RH37 (11 peptides), RH52 (eight peptides), annexin1 (ANN1, 23 peptides), and ANN2 (16 peptides) (Fig. 1a and Supplementary Table 2). RH11, RH37 and RH52 belong to the same clade of DEAD-box RHs, and share more than 80% homology. Because MS analysis identified five peptides specific to RH11, three specific to RH37 and none specific to RH52, we chose to mainly study the function of RH11 and RH37. To confirm the proteomics results experimentally, we conducted western blot analyses on proteins isolated from EVs. For the RBPs lacking native antibodies, we generated transgenic fluorescence protein-tagged Arabidopsis plants, including RH11-CFP, RH37-CFP and ANN1-YFP lines. AGO1, RH11, RH37, ANN1 and ANN2 were easily detected in isolated Arabidopsis EVs (P100) (Fig. 1b), whereas AGO2, AGO4 and AGO5 were not present in EVs (Fig. 1b). This result is consistent with the proteomics result (Supplemental Table 2). The EV-associated TET8 marker was used as a positive control and the MVB marker ARA6 and the trans-Golgi marker SYP61 were used as

107

108

109

110

111

112

113

114

115

116

117

118

119

120

121

122

123

124

125

126

127

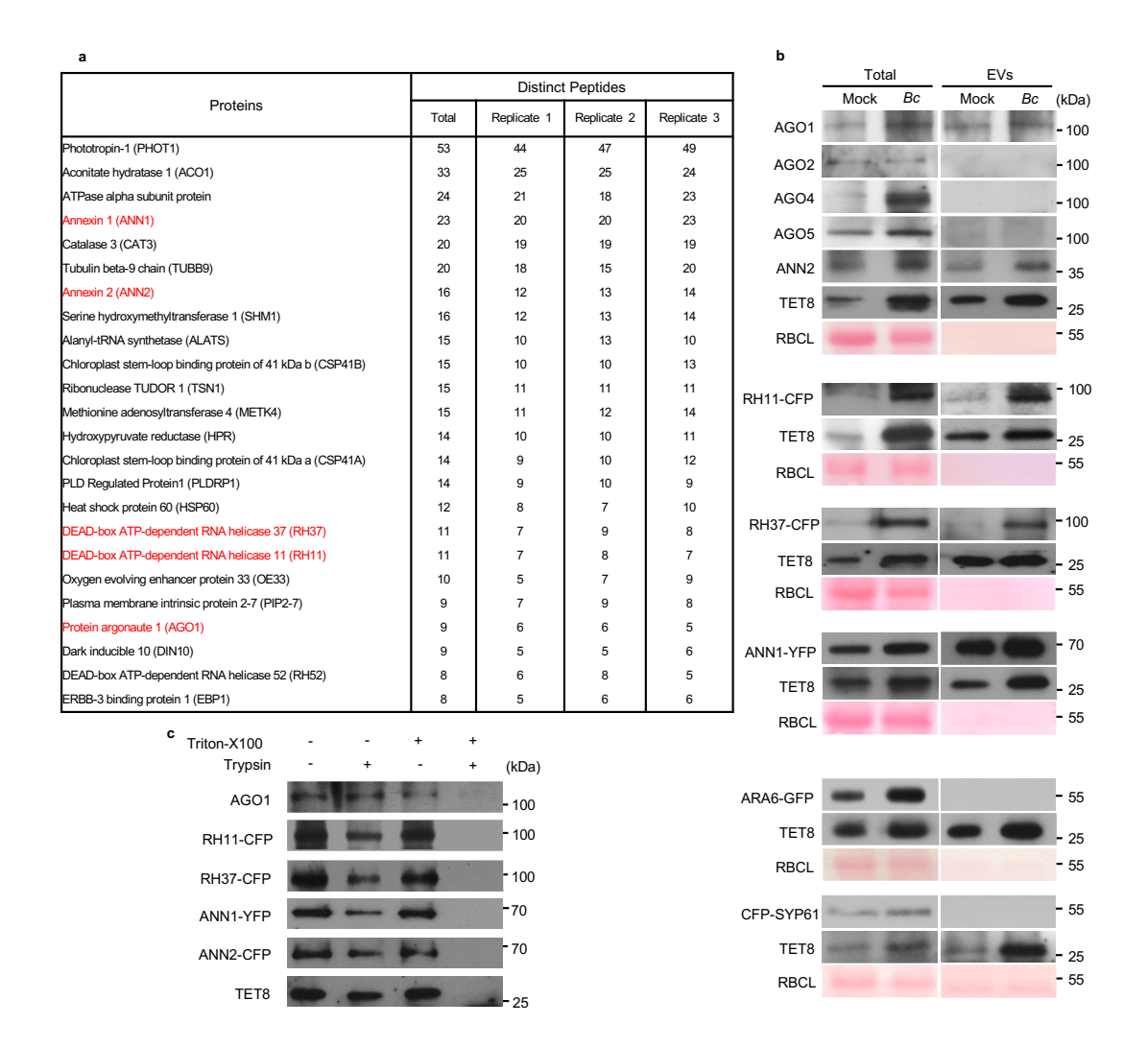
negative controls to ensure that the isolated EVs were not contaminated by plasma membrane or other endomembrane fractions (Fig. 1b). To further confirm that these RBPs were located inside EVs, not just adhered to the outer surface of EVs, the isolated EVs (P100) from *Arabidopsis* leaves were subjected to trypsin digestion in the presence or absence of Triton-X100, a detergent that can rupture EVs. These RBPs were still detected in EVs after trypsin treatment, while the combination of Triton-X100 and trypsin completely digested them (Fig. 1c). These results indicate that AGO1, RH11, RH37, ANN1 and ANN2 are secreted by EVs in plants.

Fig. 1

RNA binding proteins present in plant EVs.

a, Candidates of RNA binding proteins detected in plant EVs. Proteins in red were chosen for further experimental analysis. b, RNA binding proteins AGO1, RH11, RH37, ANN1 and ANN2 can be detected from purified EVs by western blot. EVs were isolated from the untreated (Mock) and *B. cinerea* infected (*Bc*) wild-type, RH11-CFP, RH37-CFP, ANN1-YFP, ARA6-GFP and CFP-SYP61 plants. AGO1, AGO2, AGO4, AGO5, ANN2 and TET8 were detected by western blot using antibodies against AGO1, AGO2, AGO4, AGO5, ANN2, and TET8, respectively. RH11-CFP, RH37-CFP, ANN1-YFP, ARA6-GFP and CFP-SYP61 were detected by western blot using antibodies against GFP. TET8, ARA6, and SYP61 were used as EV, MVB and trans-Golgi Network markers, respectively. To perform the western blot, 20 μg of total and 10 μg of EV proteins were used. Ponceau-S staining of Rubisco was used as the loading control. c, Trypsin digestion of plant EVs. EVs were isolated from wild-type, RH11-CFP, RH37-

CFP, ANN1-YFP and ANN2-CFP plants and incubated with 1% Triton-X100, with 10 µg ml⁻¹ of trypsin, or a combination of both, for 30 min at 37 °C. Samples were analysed by western blot with antibodies against AGO1, TET8 and GFP, respectively. The experiments in **b** and **c** were repeated three times with similar results. Source data



Secreted RBPs are enriched in TET8 -positive EVs

In mammalian systems EVs are divided into multiple subclasses on the basis of the associated protein markers and their biogenesis pathways, and it is likely that plants also possess distinct subclasses of EVs. In addition to TET8-positive EVs ⁴, Rutter and

Innes have identified PENETRATION 1 (PEN1)-positive EVs from Arabidopsis, which are enriched in the 40,000g (P40) ultracentrifugation fraction ²⁴. To determine whether TET8-positive EVs and PEN1-positive EVs are distinct subclasses of plant EVs, we generated transgenic plants co-expressing two fluorescence-tagged fusion proteins TET8-GFP and mCherry-PEN1. Numerous distinct GFP-labelled EVs and mCherrylabelled EVs were observed in the leaf apoplast fluid from the transgenic plants (Fig. 2a). TET8-GFP labelled EVs were not colocalized with mCherry-PEN1-labelled EVs, indicating that these are two distinct subclasses of plant EVs. Consistent with previous results ^{4, 24}, TET8-positive EVs and PEN1-positive EVs were enriched in the P100 and P40 fractions, respectively (Fig. 2a,b). Furthermore, a substantial amount of TET8positive EVs were isolated after centrifugation of the supernatant of fraction P40 at 100,000g (P100-40), which was largely depleted of PEN1-positive EVs (Fig. 2a,b). Further, secreted sRNAs were more concentrated in the P100 fraction than in the P40 fraction (Fig. 2c). We previously demonstrated that TET8 colocalized with *Arabidopsis* MVB marker Rab5-like GTPase, ARA6, inside the plant cell, suggesting that TET8positive EVs are derived from MVBs and could be considered plant exosome-like EVs 4. However, our observations indicate that PEN1 does not colocalize with ARA6marked MVBs (Extended Data Fig. 3), suggesting that the PEN1- and TET8-positive EVs have distinct biogenesis pathways. These results support the suggestion that plants secrete different subtypes of EVs with distinct biomarkers and biogenesis pathways.

181 **Fig. 2**

161

162

163

164

165

166

167

168

169

170

171

172

173

174

175

176

177

178

179

180

182

TET8 and PEN1 label different classes of EVs in Arabidopsis.

a, Confocal microscopy of EVs isolated from B. cinerea-infected TET8-GFP/mCherry-PEN1 double fluorescence plants by ultracentrifugation at 40,000g (P40 fraction) and 100,000g (P100 fraction) for 1 h. For the P100-40 fraction, the supernatant of P40 fraction was centrifuged at 100,000g for 1 h. Scale bars, 10 µm. b, Detection of GFPlabelled TET8 and mCherry-labelled PEN1 in P40, P100, and P100-40 EV fractions by western blot. c, EV-enriched sRNAs were detected in P40, P100, and P100-40 EV fractions by real-time-RT PCR. The data are presented as mean \pm s.d., n = 3 biological replicates. The error bars represent s.d. d, Six fractions were collected from top-loading plant EV sucrose gradient centrifugation and analysed for protein content by western blot and for sRNAs by RT-PCR. AGO1, AGO2, AGO4, RH11, RH37, ANN1, ANN2 and TET8 proteins were examined by western blot. EV-enriched sRNAs (TAS1csiR483, TAS2-siR453 and miR166), non-EV-associated sRNAs (TAS1c-siR585 and TAS2-siR710), AGO2-associated miR393* and AGO4- associated siRNA1003 were examined by RT-PCR. All EVs used here were not pretreated with trypsin and RNase. The statistical analysis was performed using ANOVA Dunnett's multiple comparisons test. The small open circles represent the individual values. *P < 0.05, **P < 0.01. NS, not significant. The experiments in a, b and d were repeated three times independently with similar results. Source data

183

184

185

186

187

188

189

190

191

192

193

194

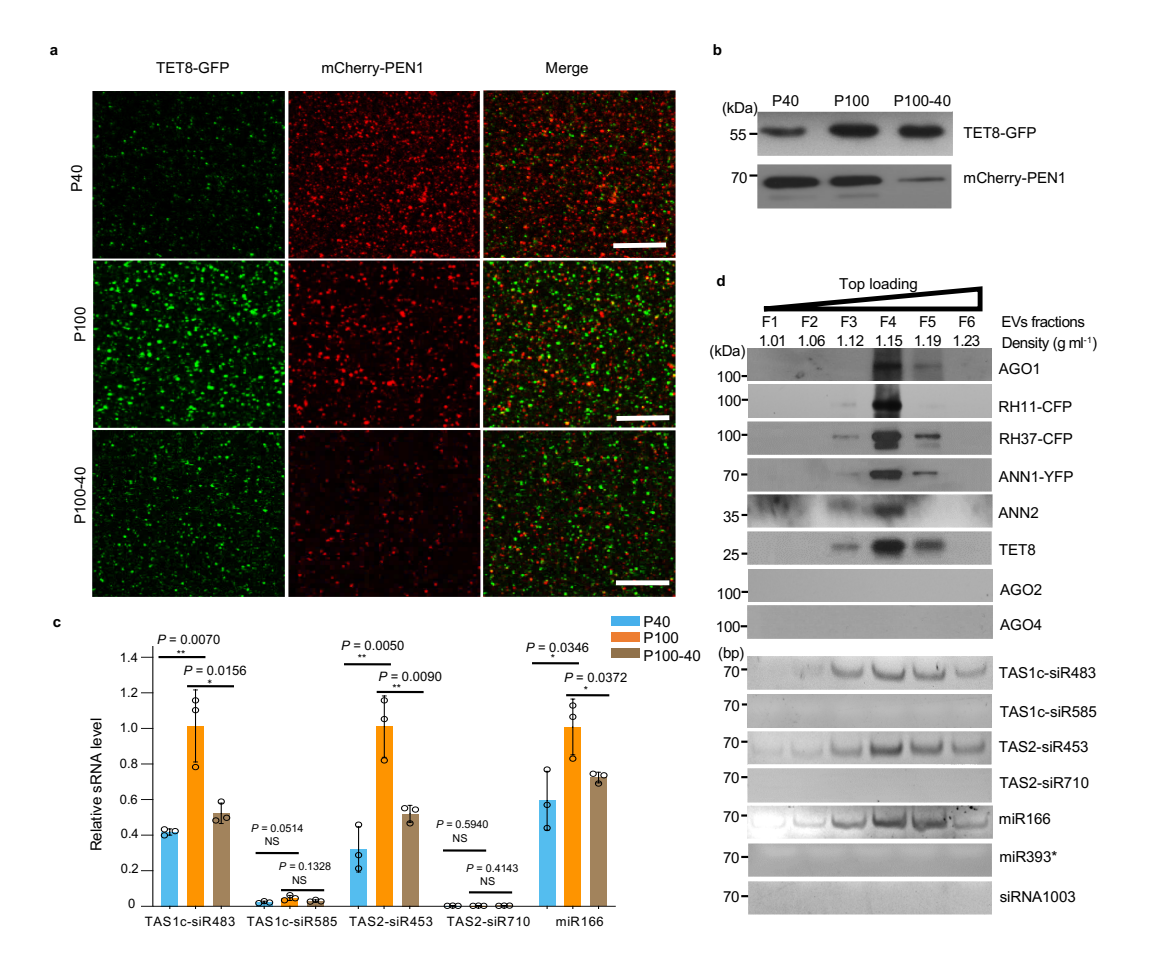
195

196

197

198

199



Since plant exosome-like EVs carry sRNAs, we hypothesize that the AGO1 protein and other identified RBPs may be also enriched in TET8-positive EVs. To test this, we performed density gradient analysis, a classical method used to separate different EVs according to their floatation speed and equilibrium density^{12, 13, 25, 26}. Isolated EVs (P100) were further separated by sucrose gradients centrifugation using both top-loading and bottom-loading methods (Extended Data Fig. 4a). EV-enriched sRNAs that we previously identified⁴ and TET8 were used to identify the TET8-positive EV fractions. As shown in Fig. 2d and Extended Data Fig. 4b, plant EV-enriched sRNAs, TAS1c-siR483, TAS2-siR453 and miR166, and TET8 are found in the EV fractions at the density of 1.12-1.19 g ml⁻¹, which is consistent with the density

of exosomes in animal systems ¹¹. As expected, the RBPs AGO1, RH11, RH37, ANN1 and ANN2 were also detected only in the fraction of TET8-positive EVs, by both top-and bottom- loading ultracentrifugation procedures (Fig. 2d and Extended Data Fig. 4b). These results suggest that sRNAs and RBPs are probably secreted in TET8-positive EVs.

218

219

220

221

222

223

224

225

226

227

228

229

230

231

232

233

234

213

214

215

216

217

Exosome-like EVs are the main subclass of plant EVs for sRNA and RBP secretion

Recent advances in methodology development for EV isolation in mammalian systems indicate that the most powerful tool to isolate pure specific subclasses of EVs is immunoaffinity capture ^{26, 27}. This method isolates a specific subclass of EVs using beads coated with an antibody that recognizes the specific protein marker exposed on EV membranes (such as exosome marker CD63) ^{25, 26, 28, 29}. To determine whether exosome-like EVs are responsible for sRNA and RBP secretion in plants, we isolated exosome-like EVs using TET8 immunoaffinity capture. Because both the amino terminus and carboxy terminus of the TET8 protein are inside of vesicles (Fig. 3a), it was not possible to use a fused GFP-tag for immunoaffinity capture of EVs. Therefore, we had to generate a native antibody that specifically recognizes the large exposed extravesicular loop, EC2 domain, of TET8 (Fig. 3a). This antibody was unable to detect any signal in the tet8 mutant background, demonstrating that it was indeed TET8specific (Fig. 3b). We successfully isolated TET8-positive EVs by direct immunoaffinity capture using this antibody (Fig. 3c). We could easily detect the EVenriched sRNAs that we previously identified 4, including TAS1c-siR483, TAS2siR453 and miR166, in the anti-TET8-captured EVs (Fig. 3d), further confirming that TET8-positive EVs are an important class of EVs for sRNA secretion. Furthermore, the RBPs AGO1, RH11, RH37, ANN1 and ANN2 were clearly detectable in the TET8-positive EVs (Fig. 3e).

Fig. 3

235

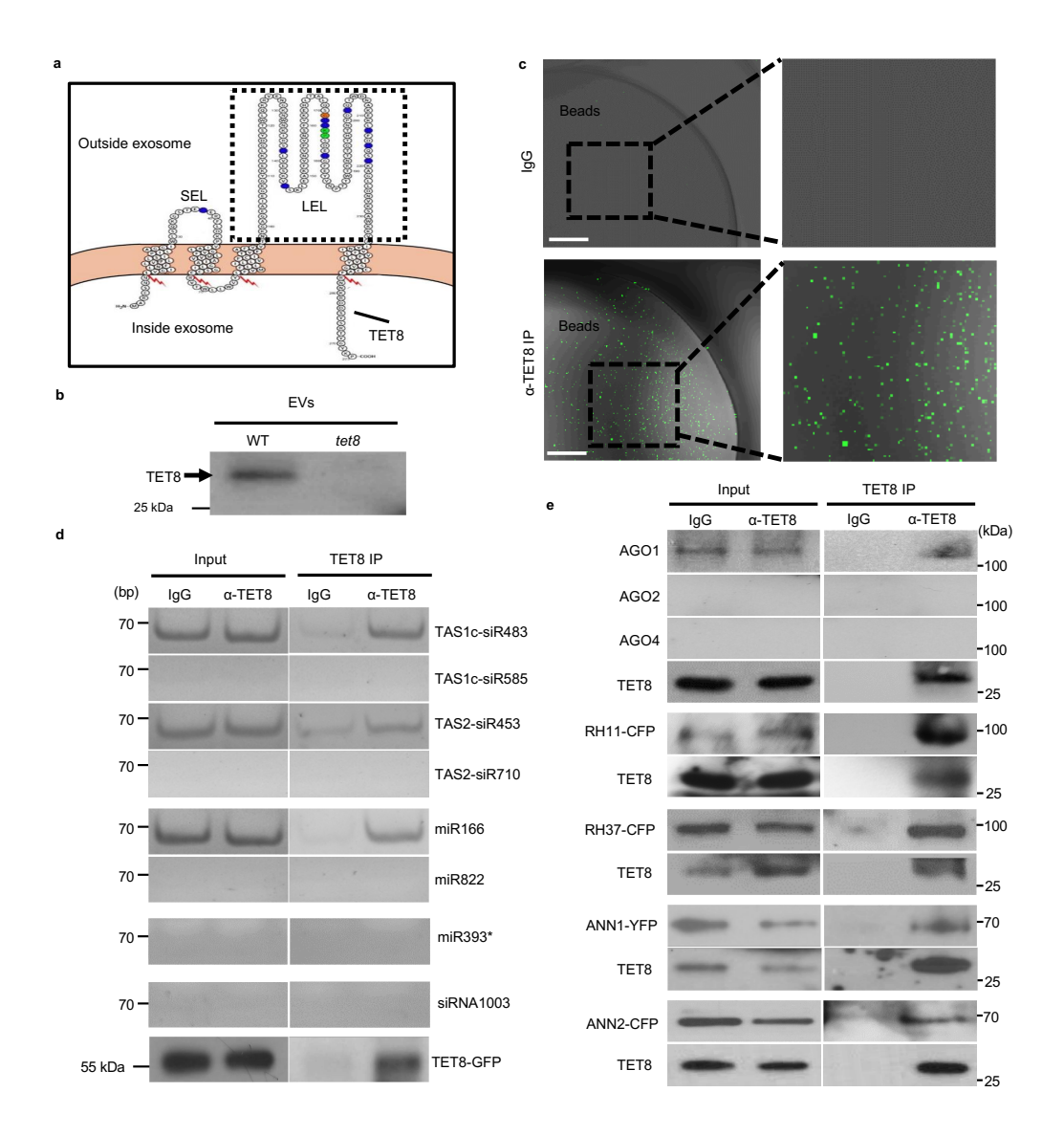
236

237

238

239

- TET8-positive EVs are an important subclass of EVs for secretion of sRNAs and
- 241 **RBPs.**
- a, The structures and the topology of plant TET8. The peptide of the large extracellular 242 loop EC2 domain was used for production of TET8-specific antibody. b, Anti-TET8 243 244 can detect TET8 in EVs isolated from wild-type plants but not from the tet8 mutant. c, TET8-positive EVs can be pulled-down by TET8-specific antibody-linked beads. IgG 245 was used as a negative control. d, EV-associated sRNAs are enriched in EVs isolated 246 from TET8-specific antibody pull-down fractions. AGO2-associated miR393* and 247 AGO4-associated siRNA1003 were not present in the TET8-positive EVs and were 248 used as negative controls. e, AGO1, RH11, RH37, ANN1 and ANN2 were detected in 249 250 anti-TET8 immuno-isolated EV fractions by western blot. AGO2 and AGO4 were not present in the TET8-positive EVs. Scale bars, 10 µm. The experiments in b, d and e 251 were repeated three times and similar results were observed. Source data 252

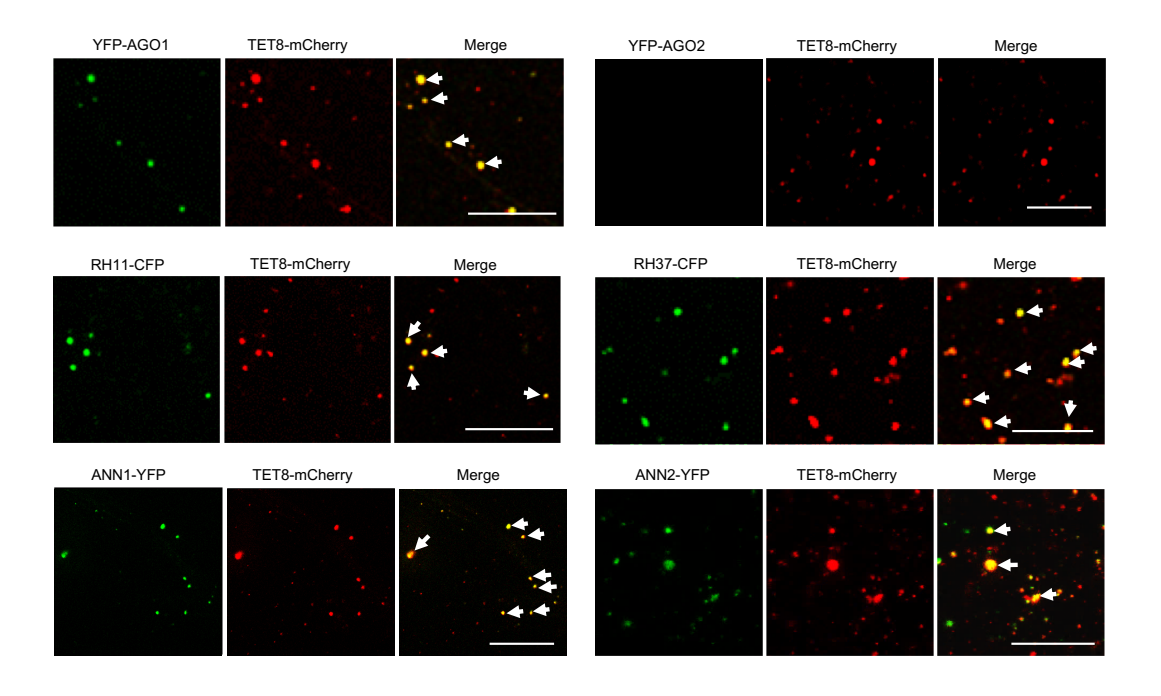


We also confirmed that these RBPs colocalized with TET8 and MVB marker ARA6 (Extended Data Fig. 5) inside the plant cells and with TET8 in the secreted EVs (Fig. 4). Colocalization of these RBPs with MVBs may facilitate their loading into EVs with their associated sRNAs. These data strongly support that these RBPs, together with sRNAs, are secreted by MVB-derived EVs, and that the subcellular localization of these RBPs facilitates their loading into exosome-like EVs.

Fig. 4

EV-associated RBPs colocalize with EV marker TET8 in isolated EVs.

Fluorescent protein-labeled RBPs were co-expressed transiently with EV marker protein TET8 in *N. benthamiana*. Confocal microscopy was used to determine the localization of RBPs with TET8 in the isolated EVs. AGO2 was used as a negative control. The arrows indicate colocalized signals of RBPs and TET8 in isolated EVs. Scale bars, 10 μm. Similar results were observed in three biological repeats.



EV-localized RBPs mediate sorting and stabilization of secreted sRNAs

The AGO1-associated tasiRNAs (TAS1c-siR483 and TAS2-siR453) and miRNAs (miR166 and miR156) that we previously identified⁴ could be easily detected in EVs, whereas AGO2-, AGO4- and AGO5-associated sRNAs were undetectable in the EV fractions (Extended Data Fig. 6). These results suggest that EV-localized RBPs, such as AGO1, may play an important role in sRNA selective loading into plant EVs because some of the identified RBPs bind to sRNAs specifically. To determine whether

identified EV-encased AGO1 and other RBPs specifically associate with secreted sRNAs, we immunoprecipitated RBPs from total cell extraction and EV extraction and analysed the copurified sRNAs. Our results showed that AGO1, RH11 and RH37 could bind specifically to EV-enriched sRNAs 4, such as miR166, TAS1c-siR483 and TAS2siR453, in both the total cell extraction and the EV extraction (Fig. 5a,b). We previously showed that TAS1c-siR585 and TAS2-siR710, which are derived from the same messenger RNA precursors as TAS1c-siR483 and TAS2-siR453, respectively, were not detected in the EVs 4. These non-EV associated sRNAs were not associated with AGO1, RH11, and RH37 in either the total cell extraction or the EV extraction (Fig. 5a,b). We also co-expressed AGO1 or RH37 with EV-enriched or non-EV sRNAs in Nicotiana benthamiana to confirm the selective binding between AGO1 and RH37 with EVenriched sRNAs. As shown in Extended Data Fig. 7, both AGO1 and RH37 can only selectively bind EV-enriched sRNAs. Because of the selective binding of EV-enriched sRNAs in the total cell extraction, AGO1, RH11 and RH37 probably bind to a specific set of sRNAs and carry them into EVs for secretion. However, ANN1 and ANN2 had no sRNA-binding specificity, they could bind both EV-enriched and non-EV sRNAs in the total cell extraction (Fig. 5a,b). These results suggest that AGO1, RH11 and RH37 function in selectively loading sRNAs into EVs, while ANN1 and ANN2 probably only contribute to the stabilization of RNA molecules in the EVs.

Fig. 5

276

277

278

279

280

281

282

283

284

285

286

287

288

289

290

291

292

293

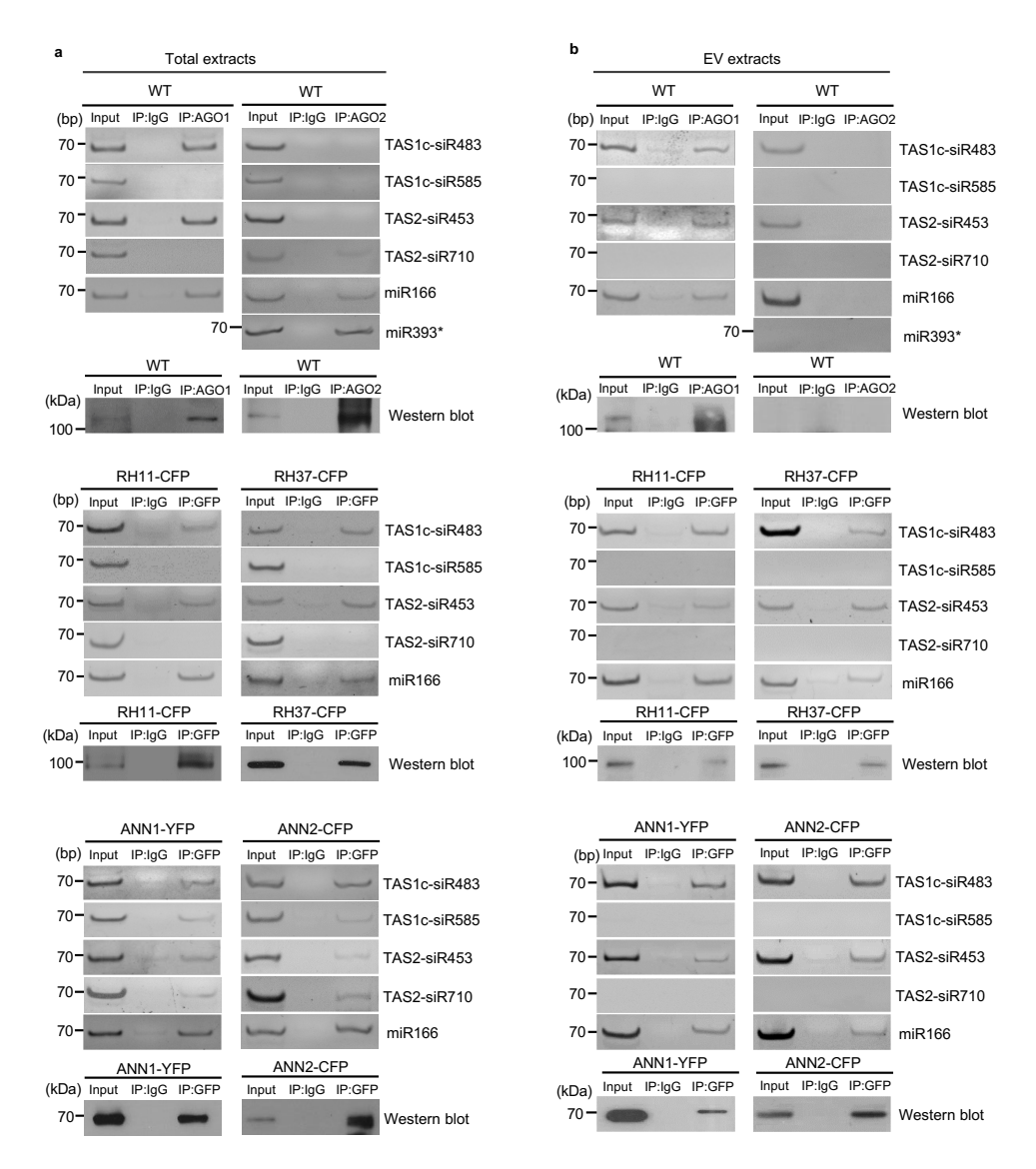
294

295

296

EV secreted RBPs mediate sorting and stabilization of sRNAs into EVs.

a, b, sRNAs were immunoprecipitated from plant total extraction (a) and EV extraction (b) using antibodies raised against AGO1, AGO2 and GFP to detect the association of EV-enriched sRNAs or non-EV-associated sRNA with AGO1, AGO2, RH11, RH37, ANN1 and ANN2. AGO1 and AGO2 proteins were detected by western blot using anti-AGO1 and anti-AGO2 antibodies, respectively. RH11, RH37, ANN1 and ANN2 were detected by western blot using anti-GFP antibody. IgG was used as a negative control. WT, wild type; IP, immunoprecipitation. The experiments in a and b were repeated three times with similar results. Source data



To genetically confirm their function in sRNA secretion, we investigated both total and EV-associated sRNA levels by both sRNA reverse transcription semi-quantitative PCR (RT-PCR) (Fig. 6a) and real-time quantitative PCR (Extended Data Fig. 9) in the ago1-27, rh11rh37, and ann1ann2 mutants. We generated the rh11rh37 double mutants by knocking down RH11 and RH37 expression with an artificial miRNA that can target both genes simultaneously in Col-0 (rh11rh37#3) or by knocking down RH37 expression in the rh11 knockout mutant background (rh11rh37#6) and generated the ann1ann2 double mutants by crossing single knockout mutants ann1 (SALK 095886C) and ann2 (SALK 205024C) (Extended Data Fig. 8). We found that the sRNA level in the EVs isolated from ago1-27, rh11rh37 and ann1ann2 was clearly decreased in comparison to wild-type plants (Fig. 6a and Extended Data Fig. 9), but the total amount of sRNAs from ago1-27, rh11rh37 and ann1ann2 was similar to wild-type plants. Furthermore, the levels of the TET8 protein in the EV fraction are similar between RBP mutants and wild type (Fig. 6a), indicating that ago1-27, rh11rh37 and ann1ann2 do not affect the secretion of TET8-positive EVs, and the reduction of EV-enriched sRNA accumulation in these RBP mutants is not due to a reduction in the amount of TET8positive EVs.

Fig. 6

306

307

308

309

310

311

312

313

314

315

316

317

318

319

320

321

322

323

324

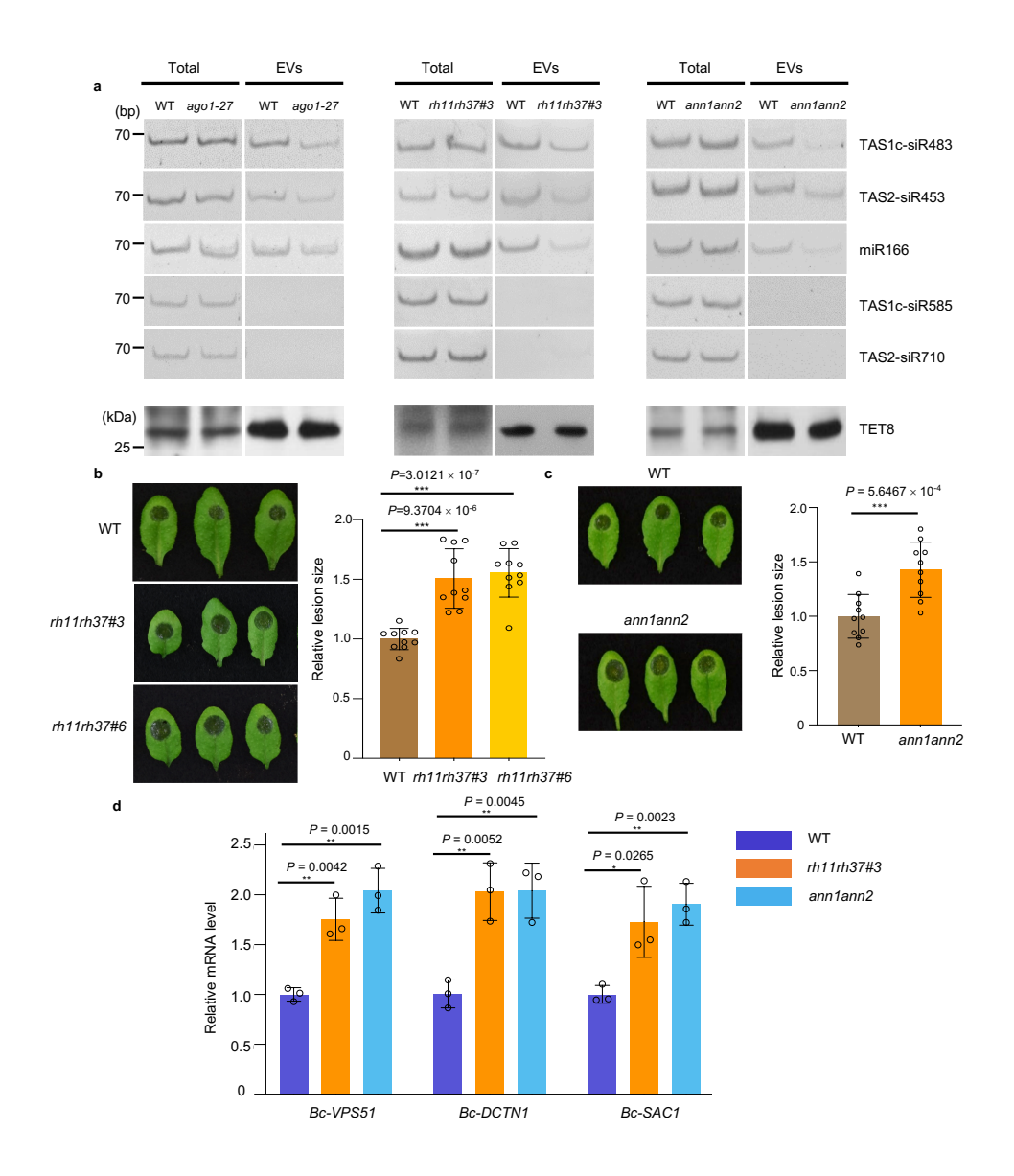
325

326

EV-associated RBPs contribute to plant immunity to fungal infection.

a, sRNAs were detected by means of sRNA semi-quantitative RT-PCR in EVs isolated from wild-type, *ago1-27*, *rh11rh37* and *ann1ann2* mutant plants. The 'total' lane

indicates total RNAs from leaves. The 'EVs' lane indicates total RNAs from isolated EV fractions. TET8 was detected by western blot using anti-TET8 antibody. Similar results were observed in three biological repeats. **b**, **c**, The *rh11rh37* (**b**) and *ann1ann2* (**c**) mutant plants exhibited enhanced susceptibility to *B. cinerea* in comparison to the wild type. Relative lesion sizes were measured 2 d after infection. The data are presented as mean \pm s.d., n = 10 biological replicates. **d**, Fungal target genes of transferred sRNAs were derepressed in *B. cinerea* collected from the *rh11rh37* and *ann1ann2* mutants. The data are presented as mean \pm s.d., n = 3 biological replicates. The statistical analysis in **b** and **d** was performed using ANOVA Dunnett's multiple comparisons test. The statistical analysis in **c** was performed using unpaired two-tailed Student's *t*-test. The small open circles represent the individual values. The error bars indicate s.d. *P < 0.05, **P < 0.01, ***P < 0.001. Source data



As EV-localized RBPs mediate selective loading and stabilization of secreted sRNAs, many of which move into fungal cells to silence fungal virulence-related genes, they are likely to contribute to plant immune responses against fungal infection. Indeed, we found that the *rh11rh37* and *ann1ann2* mutants were more susceptible to *B. cinerea* in comparison to wild-type plants (Fig. 6b,c). Meanwhile, the expression of fungal virulence-related genes that are targeted by plant secreted sRNAs were derepressed in *B. cinerea* that collected from the *rh11rh37* and *ann1ann2* mutants (Fig. 6d). These

results support the idea that EV-localized RBPs contribute to host immunity, probably by sorting and stabilizing fungal gene-targeting sRNAs in EVs.

350

351

352

353

354

355

356

357

358

359

360

361

362

363

364

365

366

367

368

348

349

Discussion

Previously, we demonstrated that plants can selectively transport sRNAs into fungal pathogens using EVs to induce cross-kingdom RNAi of fungal virulence-related genes ⁴. However, the mechanisms of selective sRNA loading and stabilization in EVs were unclear. Although mammalian EV studies suggest that some RBPs are involved in sRNA loading into EVs, different RBPs were identified in different cell lines or systems and a conclusive mechanism is still lacking 16, 17, 30-32. In this study, we identified several RBPs in plant EVs, including the AGO1 protein, RHs, and ANNs. They are colocalized with the endosomal MVB marker ARA6 and are probably packaged into MVB-originated exosomes with their associated sRNAs. We further demonstrate that AGO1, RH11 and RH37 bind to EV-enriched sRNAs in the total cell extraction. In the ago1-27 and rh11rh37 mutants, the abundance of EV-enriched sRNAs was reduced. These results suggest that these EV-encased RBPs probably contribute to selective sRNA sorting and stabilization within EVs. Annexins are traditionally viewed as Ca²⁺- and lipid-binding proteins, but there is more and more evidence of their role in RNA binding. Human Annexin A2 (ANXA2) interacts with mRNAs through its C-terminal helices C and D in domain IV ³³, it also regulates the loading of miRNAs into EVs in a sequence-independent manner ¹⁸. Arabidopsis ANN1

and ANN2 bind to both EV-enriched and non-EV-associated sRNAs in total cell extraction but EV-associated sRNAs were reduced in the *ann1ann2* double mutant, suggesting that they do not play a role in selective sRNA loading into EVs but stabilizing sRNAs within EVs.

369

370

371

372

373

374

375

376

377

378

379

380

381

382

383

384

385

386

387

388

389

390

Studies of mammalian EVs exhibit contradictory results on the role of AGOs in exosomal miRNA sorting 34-36. For example, in colon cancer cell lines, AGO2 was found in exosomes and the knockdown of AGO2 leads to the decrease of specific miRNAs in exosomes 34, although mammalian AGOs bind miRNAs and siRNAs indiscriminately of sequence ³⁷⁻³⁹. Why selective miRNA loading was affected is still not understood. Discordantly, other studies reported that EVs do not contain AGO2 and it was found to carry and stabilize a population of non-vesicle-associated miRNAs in human plasma ⁴⁰. To date, the function of AGOs in sRNA selection and loading into EVs is still not clear. In plants, however, AGOs have distinct binding preferences to sRNAs with specific 5'-terminal nucleotides and duplex structures ^{20,21}. Here we show that AGO1 is secreted in plant EVs and binds specifically to 20-22-nucleotide sRNAs with 5'-terminal U, suggesting that AGO1 is probably responsible for the selective loading of at least some of the sRNAs in EVs. In animals, MVBs associate with components of miRNA effector complexes, including AGO2, and modulate miRNA activity⁴¹. Arabidopsis AGO1 was shown to be enriched in the endoplasmic reticulum ⁴² and MVBs (Extended Data Fig. 5). Our data demonstrate that its subcellular compartmentation allows AGO1, with its selectively associated sRNAs, to be efficiently loaded into MVB-derived exosomes.

Increasing evidence suggests that animal EVs are made up of heterogeneous populations of vesicles¹⁵, including exosomes, microvesicles and apoptotic bodies ⁹. RNAs and RNA binding proteins have been found in different classes of EVs isolated from different cells and tissues ^{43,31}. Plants have at least three subclasses of EVs: TET8positive EVs, PEN1-positive EVs and exocyst positive organelle (EXPO)-derived EVs⁴, ^{24,44}, indicating that EV heterogeneity also exists in plants. But whether PEN1-positive EVs and EXPO-derived EVs are also involved in cross-kingdom RNAi remains to be discovered. Here, we used sucrose density gradient centrifugation and immunoaffinity purification methods to isolate TET8-positive EVs and confirmed that RBPs and sRNAs are enriched in TET8-positive EVs. Recently, animal exosomes have been implicated in transporting various sRNAs between cells within an organism 11-14, 45 or between organisms ^{46, 47}. Thus, sRNA secretion through exosomes or exosome-like EVs has evolved in both plant and animal systems and is probably a conserved mechanism for cell-to-cell communication within an organism as well as communications between interacting organisms. This study helps to elucidate the underlying molecular mechanisms of RNA-based communication and sRNA-mediated gene regulation between different organisms. A better understanding of EV-mediated sRNA trafficking will aid in the development of RNA-containing vesicles as new generation of fungicides and antifungal drugs against crop and potential human pathogens.

391

392

393

394

395

396

397

398

399

400

401

402

403

404

405

406

407

408

Methods

410

411

Plant materials

Arabidopsis thaliana ecotype Col-0 was used in this study. Arabidopsis marker lines 412 $TET8_{pro}$::TET8- $GFP^{4,48}$, $35S_{pro}$::ARA6- GFP^{4} , $SYP61_{pro}$::CFP- $SYP61^{49}$, single mutant 413 ago1-27⁵⁰ and tet8 (SALK 136039C), were used as described previously. 414 The ann1ann2 double mutant was generated by crossing the respective homozygous 415 single knockout mutants ann1 (SALK 095886C) and ann2 (SALK 205024C), which 416 were ordered from the Arabidopsis Biological Resource Center (ABRC). The rh11rh37 417 418 double mutants were generated by suppressing RH11 and RH37 with an artificial miRNA in Arabidopsis Col-0 or by suppressing RH37 in rh11 knockout mutant. The 419 rh11 knockout mutant line CS423310 was ordered from ABRC. For 35S_{pro}::ANN1-YFP, 420 35S_{pro}::ANN2-CFP, 35S_{pro}::RH11-CFP and 35S_{pro}::RH37-CFP lines, the full length 421 CDS of ANN1, ANN2, RH11 and RH37 were cloned into the pENTR vector (Life 422 Technologies), then into the destination vector pEARLYGATE 101 for YFP tagging 423 and pEARLYGATE 102 for CFP tagging, respectively. All constructs were introduced 424 into Arabidopsis Col-0 separately to generate 35S_{pro}::ANN1-YFP, 35S_{pro}::ANN2-CFP, 425 35S_{pro}::RH11-CFP and 35S_{pro}::RH37-CFP lines. For TET8/PEN1 double fluorescence 426 lines, fragments expressing mCherry-tagged PEN1 were generated by overlapping PCR. 427 These fragments were cloned separately into the pENTR vector (Life Technologies), 428 then into the destination vector pK2GW7 using Gateway LR clonase (Life 429 Technologies). Constructs for expressing mCherry-tagged PEN1 were introduced into 430

the *35S_{pro}::TET8-GFP* background ⁴⁸ to generate the double fluorescence lines. Primer sequences are provided in Supplementary Table 3.

Plant EV isolation

431

432

433

434

435

436

437

438

439

440

441

442

443

444

445

446

447

448

449

450

451

Plant EVs were isolated from *Arabidopsis* or *N. benthamiana* apoplastic wash. Plant leaves (for Arabidopsis ~100 4-week old plants, for N. benthamiana ~50 4-week old plants) were harvested and vacuumed with infiltration buffer (20 mM MES hydrate, 2 mM CaCl₂, 0.1 M NaCl, pH 6.0) and centrifuged for 10 min at 900g to collect the apoplastic fluids. The cellular debris in apoplastic fluids were removed by centrifugation at 2,000g for 30 min, followed by filtration through a 0.45-µm filter. Next, the apoplastic wash was further purified by centrifugation for 30 min at 10,000g, the supernatants were then transferred to new ultracentrifuge tubes and centrifuged for 1 h at 100,000g to obtain the P100 pellet or 40,000g to obtain the P40 pellet. The supernatants of P40 were centrifuged for 1 h at 100,000g to obtain the P100-40 pellet. The pelleted material was washed with filtered infiltration buffer at 100,000g for 1 hour to collect the pellet. To detect the protein levels in P40, P100 and P100-40 fractions, two equal parts of apoplastic wash isolated from TET8-GFP/mcherry-PEN1 were centrifuged to obtain (P40, P100-40) and (P100) respectively. After getting each fraction, the same amount of SDS-loading buffer (200 ul) was used for resuspension of the pellet, and then the same amount of sample (10 ul) was loaded into each lane for western blots. AGO1, AGO2, AGO4, AGO5 ANN2 and TET8 were detected by western blot using antibodies against AGO1 (1:2000 dilution), AGO2 (1:2000 dilution),

AGO4 (1:2000 dilution), AGO5 (1:1000 dilution), ANN2 (1:2000 dilution) and TET8 (1:2000 dilution), respectively. TET8-GFP, RH11-CFP, RH37-CFP, ANN1-YFP, ARA6-GFP and CFP-SYP61 were detected by western blot using antibodies against GFP (1:2000 dilution). mCherry-PEN1 was detected by western blot using antibodies against mCherry (1:2000 dilution).

Trypsin treatment

EVs (40 μl per treatment) were resuspended in PBS buffer, trypsin solution (Sigma) was added into EVs to the final concentration of 10 μg ml⁻¹, or Triton-X100 (Sigma) to the final concentration of 1%, or a combination of both trypsin and Triton-X100. EVs were incubated at 37°C for 30min and samples were analysed by western blot with antibodies against AGO1, GFP and TET8, respectively.

Sucrose gradient separation of EVs

Plant EVs were purified by discontinuous sucrose density gradient centrifugation. We prepared 10-90% sucrose stocks (w/v), including 10, 16, 22, 28, 34, 40,46, 52, 58, 64, 70, and 90%, using infiltration buffer (20 mM MES hydrate, 2 mM CaCl₂, 0.1 M NaCl, pH 6.0). The discontinuous gradient was prepared by layering 1 ml of each solution in the 15 ml ultracentrifuge tube. For top loading, the P100 fraction (in 100 μl infiltration buffer) was premixed with 1 ml of 10% sucrose stock. Afterward, samples were centrifuged in a swinging-bucket rotor for 16 h at 100,000g, 4 °C and six fractions (2 ml each) were collected. For bottom loading, the P100 fraction was premixed with 1 ml of 90% sucrose stock, then centrifuged in a swinging-bucket rotor for 72 h at 100,000g,

4 °C and six fractions (2 ml each) were collected. Collected fractions were transferred to new ultracentrifuge tubes and each sample was diluted to 12 ml using infiltration buffer, followed by a final centrifugation for 1 h at 100,000g, 4 °C to obtain pellet for further analysis.

Immuno-isolation of EVs

For TET8-EV immuno-isolation, protein A beads (Roche) were coupled to antibodies either rabbit polyclonal anti-Arabidopsis TET8 (homemade) or rabbit immunoglobulin G (Thermo Fisher)) in IP buffer (20 mM MES hydrate, 2 mM CaCl₂, 0.1 M NaCl, adjust pH to 7.5). Beads were then washed with IP buffer (containing 0.3% BSA). Plant EVs were resuspended in IP buffer and then added into beads, followed by overnight incubation at 4 °C. Bead-bound EVs were collected and washed by IP buffer. RNA was extracted from the bead-bound EVs with Trizol reagent (Invitrogen). For detecting proteins, the bead-bound EVs were boiled with SDS-loading buffer and resolved in an SDS-polyacrylamide gel electrophoresis (SDS-PAGE) gel.

Immunoprecipitation

Anti-GFP (Invitrogen, Rabbit polyclonal antibody) was used to immunoprecipitate RH11, RH37, ANN1 and ANN2 from *35Spro::RH11-CFP*, *35Spro::RH37-CFP*, *35Spro::ANN1-YFP* and *35Spro::ANN2-CFP* lines. Anti-AGO1 and AGO2 (home-made, rabbit polyclonal antibody) were used to immnoprecipitate AGO1 and AGO2 from *Arabidopsis* Col-0 plants. Rabbit immunoglobulin G (Thermo Fisher) was used as a control. Before being coupled with the antibody, the Protein A beads (Roche) were

blocked in IP extraction buffer (20 mM Tris–HCl at pH 7.5, 150 mM NaCl, 5 mM MgCl₂, 1 mM DTT, 0.5% NP40, proteinase inhibitor cocktail; Sigma) containing 1% BSA and 0.1 mg ml⁻¹ RNA from yeast (Sigma) for 1 hour at 4 °C. The beads were coupled with antibodies in IP extraction buffer and then washed with IP extraction buffer (containing 1% BSA and 0.1 mg ml⁻¹ RNA from yeast). Plant total and EV extraction were lysed by IP extraction buffer and then added into antibody-coupled beads, followed by overnight incubation at 4 °C. The bead-bound protein-RNA complex was collected and washed by IP extraction buffer. For immunoprecipitation of ANN1 and ANN2, IP extraction buffer containing 1 mM CaCl₂ was used. RNA was extracted from the bead-bound EVs with Trizol reagent (Invitrogen). For detecting proteins, the bead-bound EVs were boiled with SDS-loading buffer and resolved in an SDS-PAGE gel.

Transient co-expression assays

Transient co-expression assays in *N. benthamiana* were performed by infiltrating 3-week-old *N. benthamiana* plants with *A. tumefaciens* (optical density OD₆₀₀ =1.0) strain GV3101 carrying the corresponding cloned binary vectors. Constructs for expressing CFP or YFP-tagged ARA6, AGO1, RH11, RH37, ANN1 and ANN2 were generated using pEarleyGate binary vectors. For the TET8-mCherry construct, fragment expression C-terminal mCherry-tagged TET8 was generated by overlapping PCR. The fragment was cloned into the pENTR vector (Life Technologies) and then into the destination vector pK2GW7 using Gateway LR clonase (Life Technologies). For the

CFP tagged PEN1 construct, overlapping PCR was used to tag PEN1 with CFP at the N-terminus and the corresponding fragment was introduced into pK2GW7 using Gateway LR clonase (Life Technologies). TAS1c-siR483, TAS1c-siR585, TAS2-siR453, TAS2-siR710 and miR166 were cloned into the pENTR vector (Life Technologies) and then into the destination vector pEarleyGate 100 to overexpress in *N. benthamiana*. Primer sequences are provided in Supplementary Table 3.

Confocal microscopy analyses

For visualization of EV-associated fluorescence in ultracentrifuge fractions, pellets were suspended in EV infiltration buffer and examined using a 40x water immersion lens mounted on a Leica TCS SP5 confocal microscope as previously described ⁴. For visualization of protein localization, *N. benthamiana* leaves that transiently coexpressed fluorescent protein labeled RBPs with ARA6 or TET8 were examined using a 40x water immersion lens on a Leica TCS SP5 confocal microscope. Lines were drawn to determine a region of interest and fluorescence intensity was determined per pixel along the region of interest.

sRNA expression analyses

RNA was extracted using the Trizol extraction method. The sRNA RT-PCR was performed as previously described⁵. The PCR products were visualized using a 12% PAGE gel. Quantitative PCR was performed with the CFX96 real-time PCR detection system (Bio-Rad) using the SYBR Green mix (Bio-Rad). Primer sequences are provided in Supplementary Table 3.

Mass spectrometry

536

537

538

539

540

541

542

543

544

545

546

547

548

549

550

551

552

553

554

555

556

EV samples were loaded onto a 12.5% SDS-PAGE gel and, after a very short separation, the gel slices containing the proteins were excised and cut into small pieces. The proteins were then reduced in-gel with dithiothreitol, alkylated with iodoacetamide, and subsequently digested with modified MS-grade trypsin (Thermo Pierce) at an enzyme/substrate ratio was 1:100 in 50 mM NH₄HCO₃ (pH 8.5) at 37 °C overnight. Subsequently, peptides were extracted from gels with a solution containing 5% acetic acid in H₂O and then 50% CH₃CN with 2.5% acetic acid in H₂O (v/v). The peptide mixture was subsequently dried in a Speed-vac. The resulting peptide samples were desalted by employing OMIX C18 pipet tips (Agilent Technologies, Santa Clara, CA). Liquid chromatography with tandem MS analyses were conducted on an Q Exactive Plus mass spectrometer equipped with an EASY-nLC 1200 system (Thermo Fisher Scientific). Raw files were searched using Maxquant v.1.5.2.8. Arabidopsis gene accession numbers for all proteins identified in our EVs fraction are provided in Supplementary Table 1. Proteins that were present in all three replicates and had an average peptide count of no less than eight were used for further analysis. The selected proteomes were categorized on the basis of GO annotation using The Arabidopsis Information Resource bulk data retrieval and analysis tool PANTHER v.14.1 (https://www.arabidopsis.org/tools/bulk/go/index.jsp).

TET8 polyclonal antibody preparation

A fragment coding 132-amino acid TET8-specific peptide, which consisted of amino

acids 99-230 of the EC2 domain protein, was cloned into the pMAL-C5X vector (NEB) to fuse with maltose binding protein (MBP) tag. The recombinant protein was expressed in *E. coli* (BL21) (Thermo Scientific) and purified using amylose resin (NEB). After MBP tag was removed by Factor Xa (NEB), the peptide was injected to produce rabbit polyclonal antibodies (prepared by Covance Antibody). The antibody (1:1,000 dilution) was tested by immunoblot analysis using total proteins and EV proteins extracted from wild-type *Arabidopsis*, which detected the target band of the expected size at 30.7 kD.

Fungal pathogen assays

The *B. cinerea* spores were diluted in 1% sabouraud maltose broth buffer to a final concentration of 1×10^5 spores ml⁻¹ for drop inoculation of 4-week-old *Arabidopsis* plants. The lesion sizes of *B. cinerea*-infected plant materials were measured and calculated using ImageJ v.1.52r software.

Statistical analysis

The statistical analyses were performed using analysis of variance (ANOVA) Dunnett's multiple comparisons test and unpaired two-tailed Student's *t*-test using GraphPad Prism v.9.0.0 software. The statistical tests and *n* numbers, including sample sizes or biological replications, are described in the figure legends. All the experiments were repeated at least three times independently, with similar results.

Reporting Summary

Further information on research design is available in the Nature Research Reporting Summary linked to this article.

- 578 Extended data is available for this paper at https://doi.org/10.1038/s41477-021-00863-
- 579 8.

594

- 580 Supplementary information The online version contains supplementary material
- available at https://doi.org/10.1038/s41477-021-00863-8.
- Peer review information Nature Plants thanks Michael Feldbrügge and the other,
- anonymous, reviewer(s) for their contribution to the peer review of this work.
- Publisher's note Springer Nature remains neutral with regard to jurisdictional claims
- in published maps and institutional affiliations.

Acknowledgements

- We thank N. Raikhel for the 35S pro::ARA6-GFP and SYP61pro::CFP-SYP61 seeds, L.
- Boavida for TET8_{pro}::TET8-GFP and 35S_{pro}::TET8-GFP seeds, and R. Hamby for
- editing the paper. This work was supported by grants from the National Institutes of
- Health (R01GM093008 & R35GM136379), the National Science Foundation
- 591 (IOS2017314) and AES-CE (PPA-7517H) to H.J., and the National Institutes of Health
- 592 (R01 ES025121) to Y.W. Q.C. is supported by funds from National Natural Science
- Foundation of China (32070288).

Author Contributions

- 595 H.J. conceived the idea and supervised the project. B.H., Q.C. and H.J. designed the
- experiments. B.H. and Q.C. performed most of the experiments and analysed data. L.Q.,
- and T.H. contributed to the functional analysis of the EV-associated RBPs. S.W.

generated the ANN2-CFP line and C.H. generated *rh11rh37* double mutant. W. M. and Y.W. performed mass spectrometry and conducted bioinformatics analysis. B.H., Q.C., and H.J. wrote the manuscript.

Data availability

The data that support the findings of this study are available in the Supplementary Information and Source Data provided with this paper or from the corresponding authors upon reasonable request. Additional data related to this study are available from the corresponding author upon request. The raw files for LC-MS/MS analyses generated during this study are available at PeptideAtlas (http://www.peptideatlas.org/PASS/PASS01572).

Competing interests

The authors declare no competing interests.

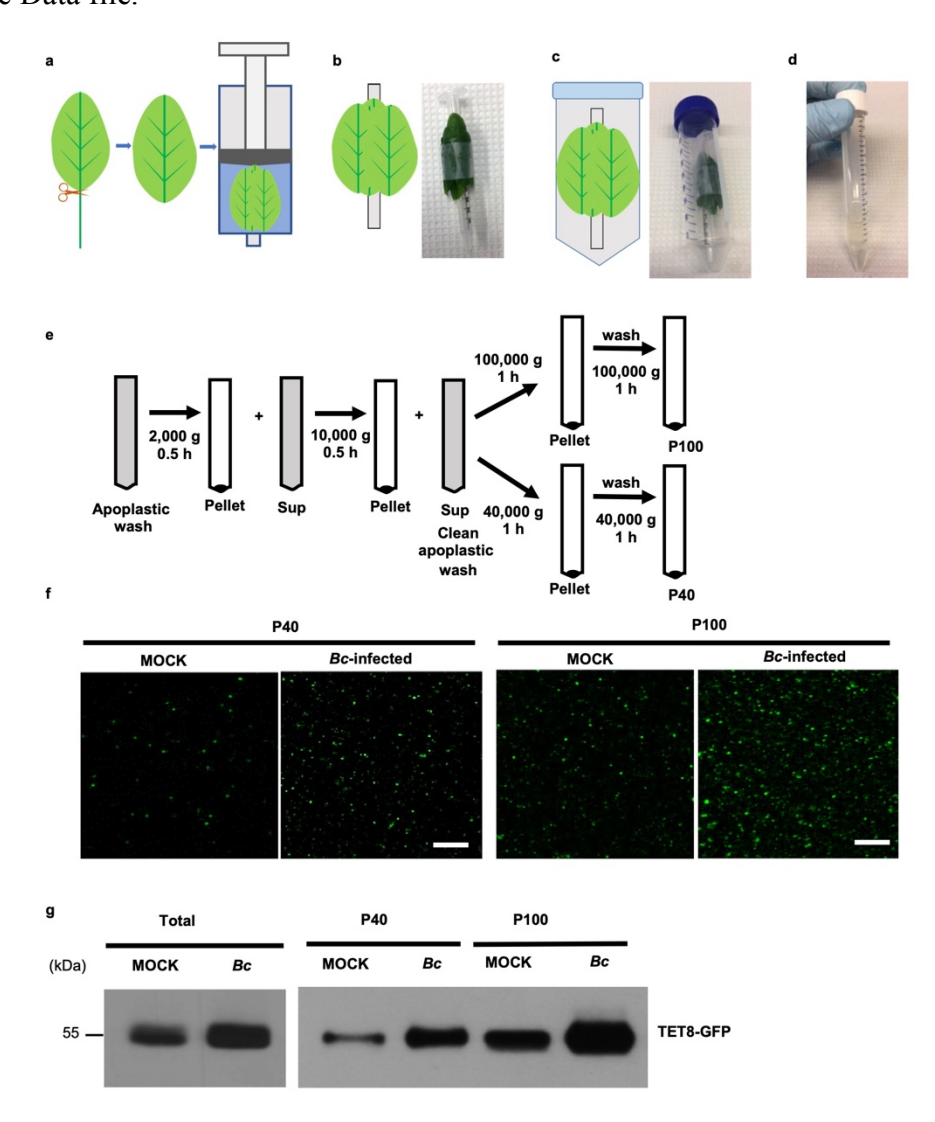
Extended data

611 Extended Data Fig.1

612 Images show the various steps in plant EVs isolation.

a, Leaves were harvested and rinsed; the petioles were removed. Next, leaves were placed in a syringe with infiltration buffer and vacuumed. **b,** The leaves were taped in the same orientation onto a 1 ml syringe after infiltration buffer was vacuumed into leaves. **c,** Syringe with taped leaves was placed into a 50 ml conical tube. **d,** The apoplastic wash was collected by gently centrifuging the leaves at 900g at 4 °C. **e,** Scheme of EV isolation by differential ultracentrifugation from apoplastic wash of *Arabidopsis*. Sup, Supernatant. **f,** Confocal microscopy images of P40 and P100 fractions isolation by ultracentrifugation from apoplastic wash of *TET8*_{pro}:; *TET8-GFP*

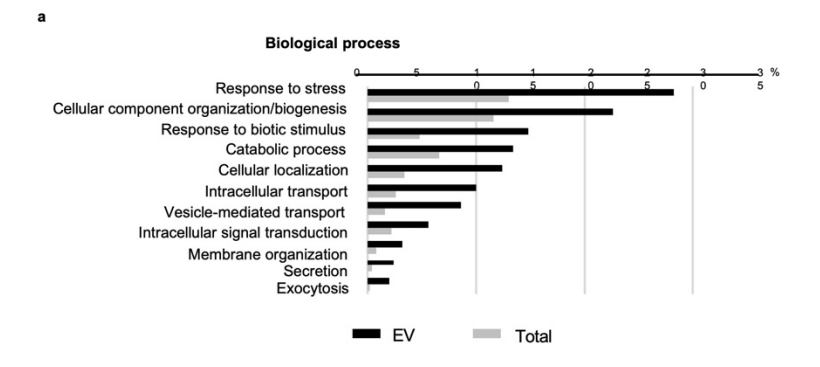
plants. Equivalent amounts of plants were inoculated with *B. cinerea* for 36 hours before P40 and P100 fraction isolation. Scale bars, 10 µm. **g**, GFP-labelled TET8 was detectable in both P40 and P100 EV fractions by western blot. The experiments were repeated three times independently with similar results. Source data are provided as a Source Data file.

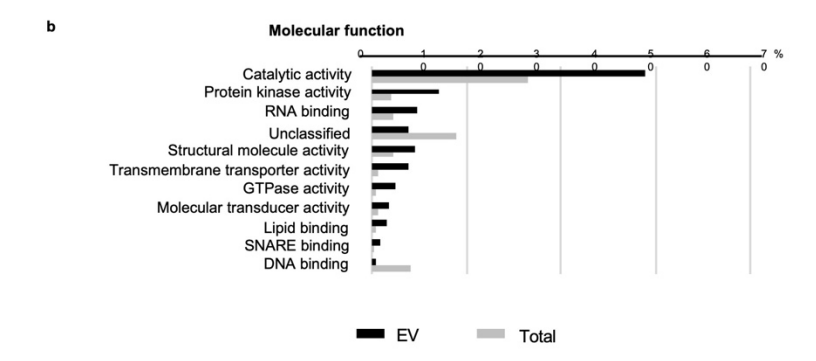


Extended Data Fig. 2

Gene ontology (GO) enrichment analysis of proteins enriched in EVs.

a, b, The plant EV proteome from B. cinerea-infected Arabidopsis plants was categorized based on GO terms related to biological process (a) and molecular function
(b) through The Arabidopsis Information Resource Web site (www.arabidopsis.org).

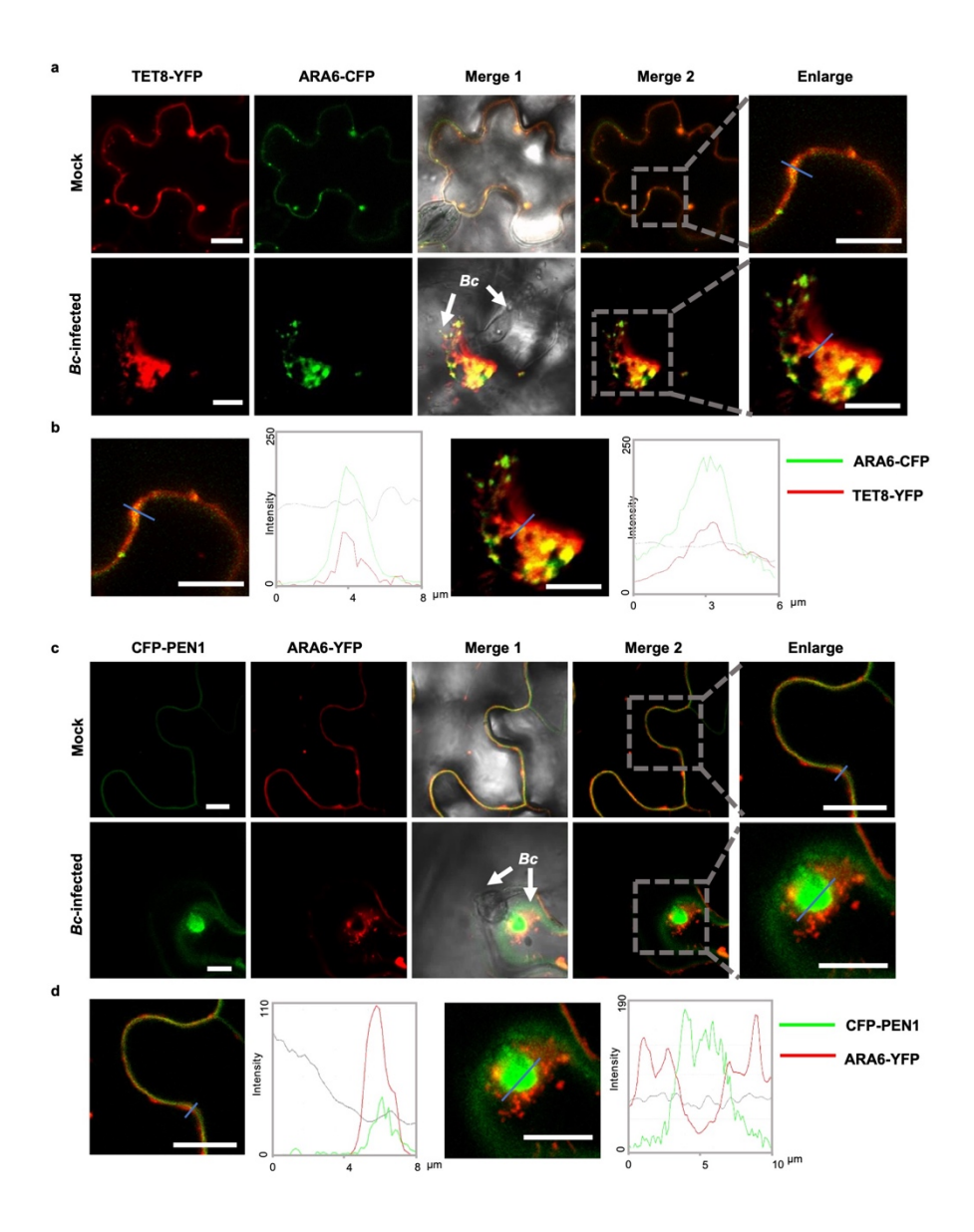




Extended Data Fig. 3

TET8 and PEN1 localization.

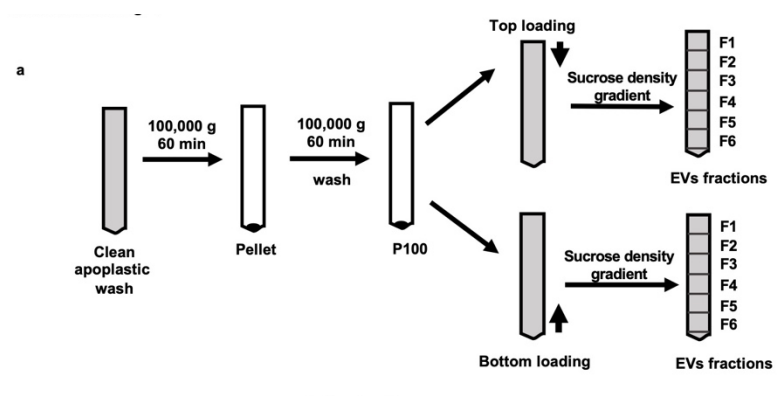
a, Confocal microscopy images of TET8-YFP and ARA6-CFP at *B. cinerea* infection site on *N. benthamiana*. TET8-YFP was partially colocalized with ARA6-CFP signals. **b,** Fluorescent intensity was quantified for the images used in (**a**). Transections used for fluorescence intensity measurements are indicated by blue lines. Green and red lines represent histograms of ARA6-CFP and TET8-YFP fluorescent intensities, respectively. **c,** Confocal microscopy images of CFP-PEN1 and ARA6-YFP at the *B. cinerea* infection site on *N. benthamiana*. CFP-PEN1 did not colocalize with ARA6-YFP signals. **d,** Fluorescence intensity was quantified for the images used in (**c**). Transections used for fluorescence intensity measurements are indicated by blue lines. Green and red lines represent histograms of CFP-PEN1 and ARA6-YFP fluorescent intensities, respectively. Scale bars, 10 μm.

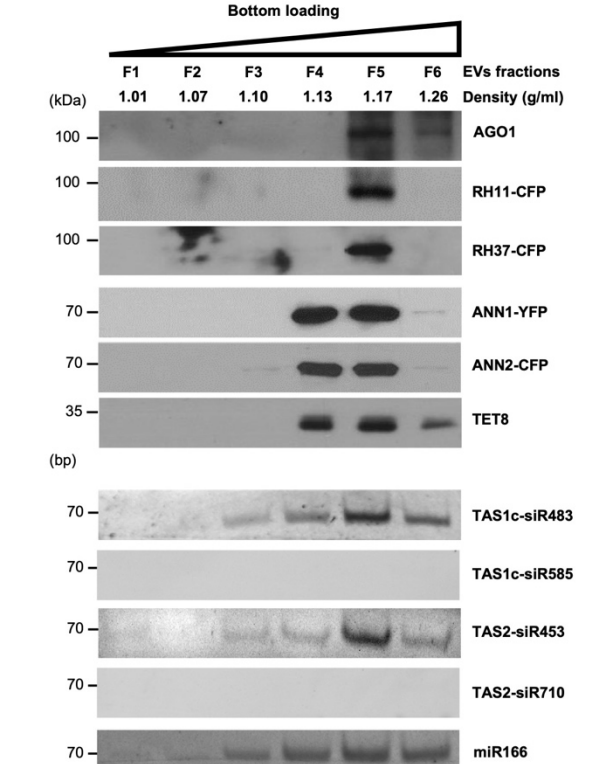


Extended Data Fig. 4

Bottom-loading EV separation by sucrose gradient centrifugation.

a, Pellets obtained from 100,000*g* centrifugations (P100) were used to perform sucrose gradient centrifugation by both top and bottom loading. **b,** Six fractions were collected from bottom-loading plant EV sucrose gradient centrifugation. TET8, AGO1, RH11, RH37, ANN1, ANN2 were detected by western blot. EV-enriched (TAS1c-siR483, TAS2-siR453 and miR166) and non-EV-associated (TAS1c-siR585 and TAS2-siR710) sRNAs were detected by RT–PCR. The experiments were repeated three times independently with similar results. Source data are provided as a Source Data file.

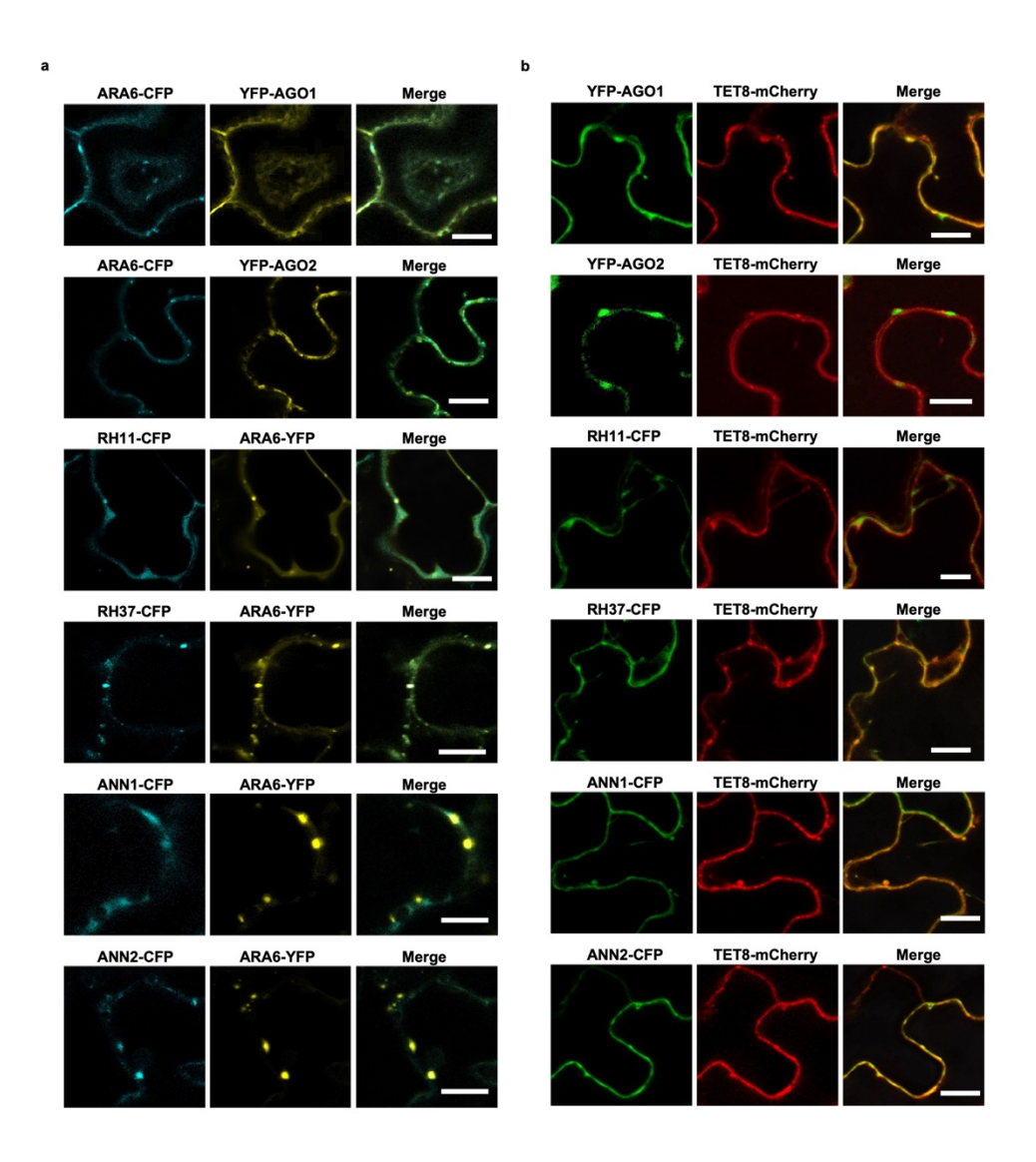




661 Extended Data Fig. 5

Colocalization between EV-associated RBPs with MVB marker ARA6 and EV marker TET8.

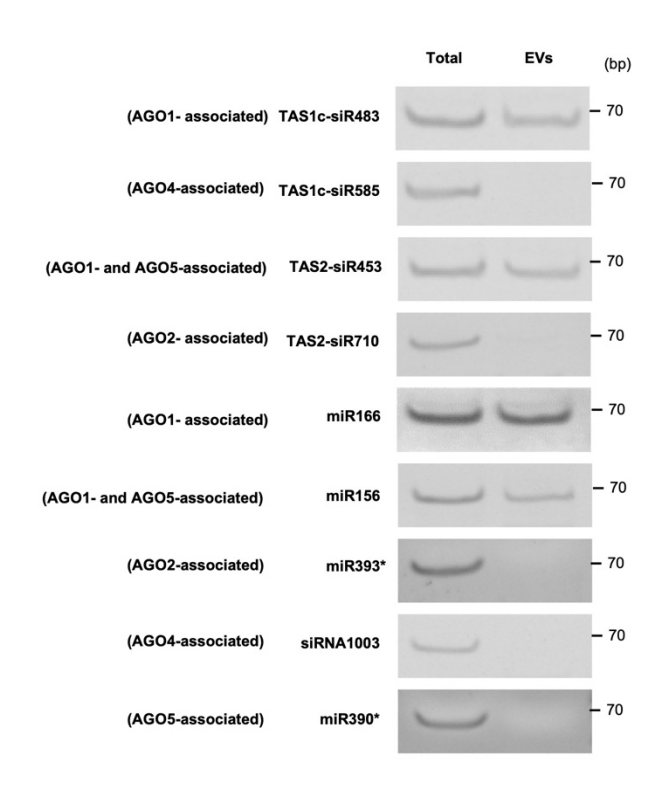
a, b, Fluorescent protein-labelled RBPs were co-expressed transiently with MVB marker ARA6 (**a**) and EV marker TET8 (**b**) in *N. benthamiana*. Confocal microscopy was used to determine the localization of RBPs (AGO1, RH11, RH37, ANN1, ANN2) with ARA6 and TET8. AGO2 was used as a control. Scale bars, 10 μm. The experiments were repeated three times independently with similar results.



Extended Data Fig. 6

sRNAs specifically bound by AGO2, AGO4 and AGO5 were absent from plant EVs.

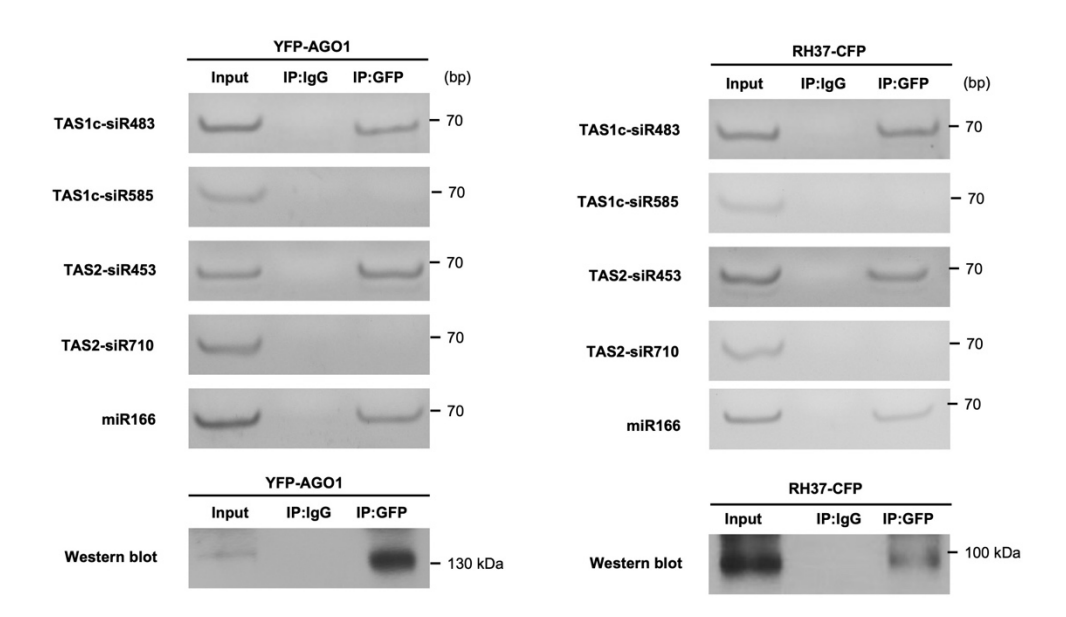
AGO2-associated miR393*, AGO4-associated siR1003, AGO5-associated miR390* and both AGO1 and AGO5-associated miR156 were examined in isolated plant EVs by sRNA RT–PCR. TAS1c-siR483, TAS2-siR453 and miR166 were detected in EVs and used as positive controls. TAS1c-siR585 and TAS2-siR710 were used as negative controls. The experiments were repeated three times independently with similar results. Source data are provided as a Source Data file.



Extended Data Fig. 7

AGO1 and RH37 selectively bind EV-enriched sRNAs in N. benthamiana.

YFP-AGO1 or RH37-CFP were co-expressed with EV-enriched (TAS1c-siR483, TAS2-siR453 and miR166) and non-EV-associated sRNAs (TAS1c-siR585 and TAS2-siR710) in *N. benthamiana*, sRNAs were immunoprecipitated from plant total extraction using antibodies against GFP and detected by sRNA RT–PCR. IgG was used as a negative control. The experiments were repeated three times independently with similar results. Source data are provided as a Source Data file.



692

693

694

695

696

697

698

699

700

701

702

703

704

705

706

707

708

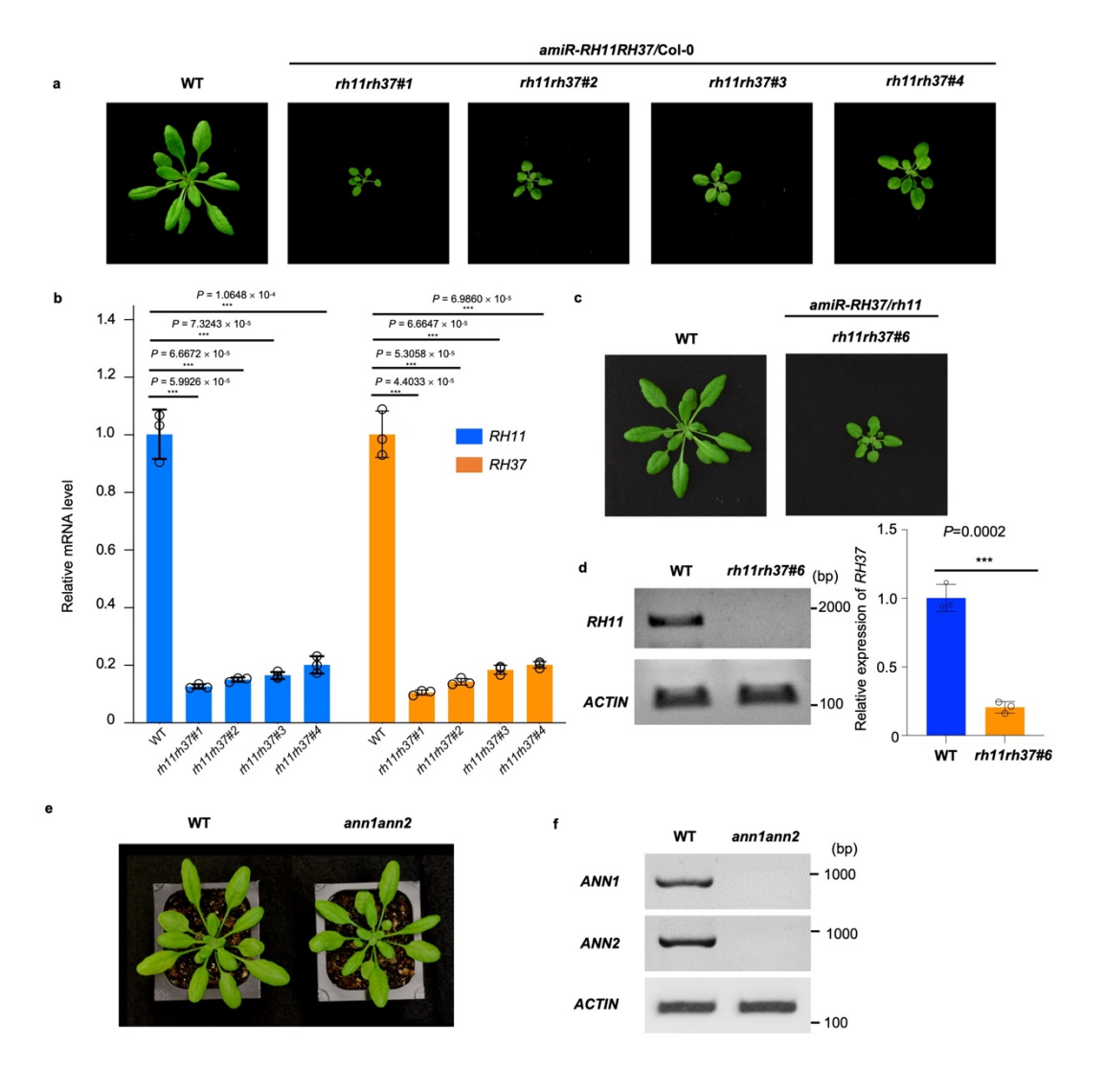
709

710

Extended Data Fig. 8

Verification of rh11rh37 and ann1ann2 double mutants.

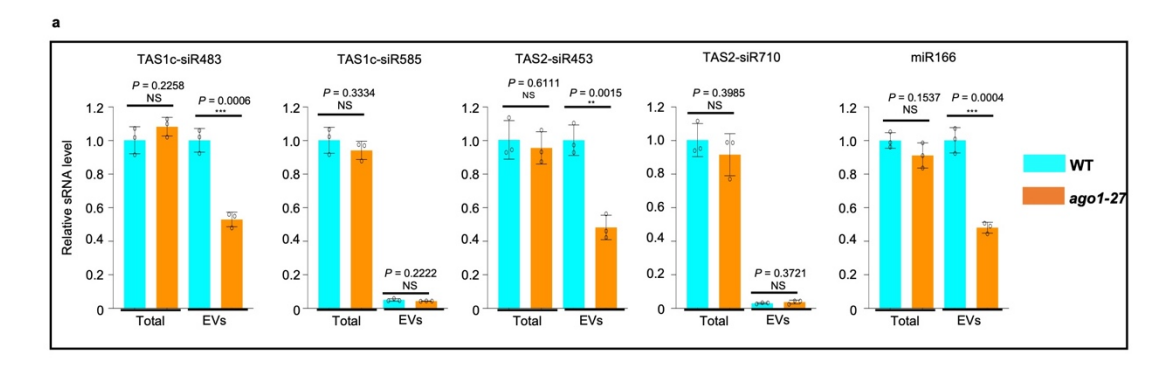
a, The developmental phenotypes of the rh11rh37 double mutant that both RH11 and RH37 expression was suppressed by artificial miRNA in Col-0. b, The real-time RT-PCR analysis of RH11 and RH37 expression in rh11rh37 mutants. The data are presented as mean \pm s.d., n=3 biologically independent replicates. The error bars indicate the standard deviation (s.d.). c, The developmental phenotypes of the rh11rh37#6 mutant that RH37 expression was suppressed by artificial miRNA in rh11 knockout mutant. d, RT–PCR analysis of RH11 and real-time PCR analysis of RH37 in rh11rh37#6 mutant. The data are presented as mean \pm s.d., n=3 biologically independent replicates. The error bars indicate the standard deviation (s.d.). e, Phenotype of wild-type and ann1ann2 mutant grown for 4 weeks in a growth chamber. f, RT-PCR analysis of the expression levels of ANN1 and ANN2 in wild-type and annlann2 double mutant. The statistical analysis in b was performed using ANOVA Dunnett's multiple comparisons test. The statistical analysis in d was performed using unpaired two-tailed Student's t-tests. The small open circles represent the individual values. The asterisks indicate significant differences: ***P < 0.001. The experiments were repeated three times independently with similar results. Source data are provided as a Source Data file.

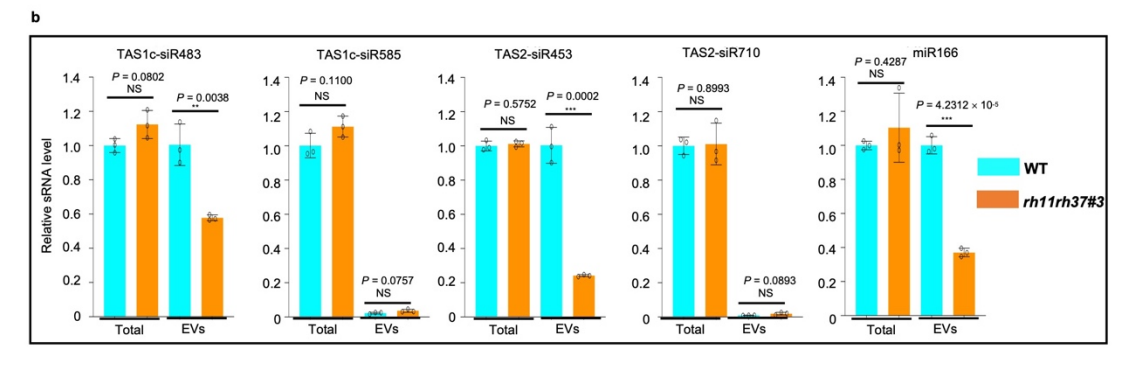


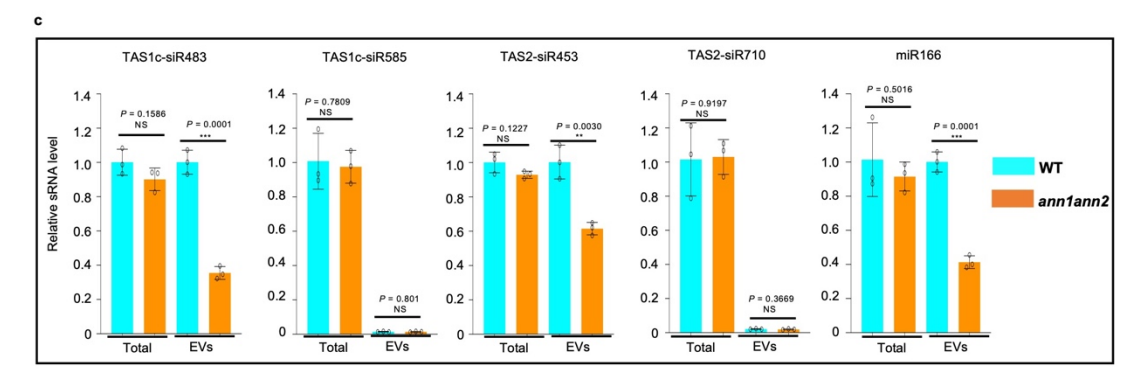
713 Extended Data Fig. 9

EV-enriched sRNA amount was reduced in EVs isolated from the mutants of EV-associated RBPs.

The relative level of both EV-enriched and non-EV-associated sRNAs were examined by quantitative real-time RT–PCR in the total fraction and EV fraction from ago1-27 (a), rh11rh37 (b) and ann1ann2 (c) mutants. The data are presented as mean \pm s.d., n=3 biologically independent replicates. The error bars indicate the standard deviation (s.d.). The statistical analysis was performed using unpaired two-tailed Student's t-tests. The small open circles represent the individual values. The asterisks indicate significant differences: **P < 0.01, ***P < 0.01, NS, not significant.







725

726

Supplementary information

Supplementary Information

- 727 Supplementary Tables 1–3.
- 728 Reporting Summary

729

730

731

732

733

734

Supplementary Tables

Supplementary Table 1. EV-associated proteins detected in all three biological replicates, with distinct peptide counts of five or more in each replicate. Related to Figure 1. Supplementary Table 2. EV-associated RBPs detected in all three biological replicates, with distinct peptide counts of five or more in each replicate. Supplementary

Table 3. Primers used in this study. 735 736 Source data 737 738 Source Data Fig. 1 739 Unprocessed western blots. 740 Source Data Fig. 2 Unprocessed western blots and gels. 741 742 Source Data Fig. 2 Statistical source data. 743 744 Source Data Fig. 3 Unprocessed western blots and gels. 745 Source Data Fig. 5 746 747 Unprocessed gels. 748 Source Data Fig. 6 Unprocessed western blots and gels. 749 Source Data Fig. 6 750 751 Statistical source data. Source Data Extended Data Fig. 1 752 753 Unprocessed western blots. Source Data Extended Data Fig. 4 754 Unprocessed western blots and gels. 755 756 Source Data Extended Data Fig. 6 Unprocessed gels. 757 758 Source Data Extended Data Fig. 7

Unprocessed gels.

759

760

761

762 **Source Data Extended Data Fig. 8**

Unprocessed western blots and gels.

Source Data Extended Data Fig. 8

763 Statistical source data.

764 Source Data Extended Data Fig. 9

765 Statistical source data.

766

767

References

- 768 1. Baulcombe, D. RNA silencing in plants. *Nature* **431**, 356-363 (2004).
- 769 2. Mello, C.C. & Conte, D., Jr. Revealing the world of RNA interference. *Nature* **431**, 338-342 (2004).
- Huang, C.Y., Wang, H., Hu, P., Hamby, R. & Jin, H. Small RNAs big players in plant-microbe interactions. *Cell Host Microbe*. **26**, 173-182 (2019).
- 773 4. Cai, Q. *et al.* Plants send small RNAs in extracellular vesicles to fungal pathogen to silence virulence genes. *Science* **360**, 1126-1129 (2018).
- Weiberg, A. *et al.* Fungal small RNAs suppress plant immunity by hijacking host RNA interference pathways. *Science* **342**, 118-123 (2013).
- Cai, Q., He, B., Weiberg, A., Buck, A.H. & Jin, H. Small RNAs and extracellular vesicles: New mechanisms of cross-species communication and innovative tools for disease control. *PLoS Pathog.* **15**, e1008090 (2019).
- 780 7. Weiberg, A. & Jin, H. Small RNAs--the secret agents in the plant-pathogen interactions. *Curr. Opin. Plant Biol.* **26**, 87-94 (2015).
- Wang, M. *et al.* Bidirectional cross-kingdom RNAi and fungal uptake of external RNAs confer plant protection. *Nat. Plants* **2**, 16151 (2016).
- 784 9. Colombo, M., Raposo, G. & Thery, C. Biogenesis, secretion, and intercellular interactions of exosomes and other extracellular vesicles. *Annu. Rev. Cell Dev. Biol.* **30**, 255-289 (2014).
- 787 10. Kowal, J., Tkach, M. & Thery, C. Biogenesis and secretion of exosomes. *Curr. Opin. Cell Biol.* **29**, 116-125 (2014).
- Valadi, H. *et al.* Exosome-mediated transfer of mRNAs and microRNAs is a novel mechanism of genetic exchange between cells. *Nat. Cell Biol.* **9**, 654-659 (2007).
- The Table 12. Lasser, C. *et al.* Human saliva, plasma and breast milk exosomes contain RNA: uptake by macrophages. *J. Transl. Med.* **9**, 9 (2011).
- Type 13. Luo, S.S. *et al.* Human villous trophoblasts express and secrete placentaspecific microRNAs into maternal circulation via exosomes. *Biol. Reprod.* **81**, 717-729 (2009).
- 797 14. Yan, W. *et al.* Cancer-cell-secreted exosomal miR-105 promotes tumour 798 growth through the MYC-dependent metabolic reprogramming of stromal 799 cells. *Nat. Cell Biol.* **20**, 597-609 (2018).
- Kowal, J. *et al.* Proteomic comparison defines novel markers to characterize heterogeneous populations of extracellular vesicle subtypes. *Proc. Natl. Acad. Sci. USA* **113**, E968-E977 (2016).
- Santangelo, L. *et al.* The RNA-Binding Protein SYNCRIP Is a Component of the Hepatocyte Exosomal Machinery Controlling MicroRNA Sorting. *Cell Rep.* **17**, 799-808 (2016).

- Shurtleff, M.J., Temoche-Diaz, M.M., Karfilis, K.V., Ri, S. & Schekman, R. Y-box protein 1 is required to sort microRNAs into exosomes in cells and in a cell-free reaction. *Elife* **5**, e19276 (2016).
- Hagiwara, K., Katsuda, T., Gailhouste, L., Kosaka, N. & Ochiya, T. Commitment of Annexin A2 in recruitment of microRNAs into extracellular vesicles. *FEBS Lett.* **589**, 4071-4078 (2015).
- 812 19. Vaucheret, H. Plant Argonautes. *Trends Plant Sci.* **13**, 350-358 (2008).
- Mi, S. *et al.* Sorting of small RNAs into Arabidopsis argonaute complexes is directed by the 5' terminal nucleotide. *Cell* **133**, 116-127 (2008).
- Zhang, X. *et al.* ARGONAUTE PIWI domain and microRNA duplex structure
 regulate small RNA sorting in Arabidopsis. *Nat. Commun.* 5, 5468 (2014).
- Linder, P. & Jankowsky, E. From unwinding to clamping the DEAD box RNA helicase family. *Nat Rev Mol Cell Biol* **12**, 505-516 (2011).
- Mingam, A. *et al.* DEAD-box RNA helicases in Arabidopsis thaliana: establishing a link between quantitative expression, gene structure and evolution of a family of genes. *Plant Biotechnol J.* **2**, 401-415 (2004).
- Rutter, B.D. & Innes, R.W. Extracellular vesicles isolated from the leaf apoplast carry stress-response proteins. *Plant Physiol.* **173**, 728-741 (2017).
- 325 25. Jeppesen, D.K. *et al.* Reassessment of exosome composition. *Cell* **177**, 428 445 e418 (2019).
- Théry, C. *et al.* Minimal information for studies of extracellular vesicles
 2018 (MISEV2018): a position statement of the International Society for
 Extracellular Vesicles and update of the MISEV2014 guidelines. *J. Extracell. Vesicles* **7**, 1535750-1535750 (2018).
- Srinivasan, S. *et al.* Small RNA Sequencing across Diverse Biofluids Identifies Optimal Methods for exRNA Isolation. *Cell* **177**, 446-+ (2019).
- Thery, C., Amigorena, S., Raposo, G. & Clayton, A. Isolation and characterization of exosomes from cell culture supernatants and biological fluids. *Current protocols in cell biology / editorial board, Juan S. Bonifacino ... [et al.]* Chapter 3, Unit 3 22 (2006).
- Xu, R., Greening, D.W., Rai, A., Ji, H. & Simpson, R.J. Highly-purified
 exosomes and shed microvesicles isolated from the human colon cancer
 cell line LIM1863 by sequential centrifugal ultrafiltration are
 biochemically and functionally distinct. *Methods* 87, 11-25 (2015).
- Chow, F.W. *et al.* Secretion of an Argonaute protein by a parasitic
 nematode and the evolution of its siRNA guides. *Nucleic Acids Res.* 47,
 3594-3606 (2019).
- Leidal, A.M. *et al.* The LC3-conjugation machinery specifies the loading of
 RNA-binding proteins into extracellular vesicles. *Nat. Cell Biol.* 22, 187 199 (2020).
- Mukherjee, K. *et al.* Reversible HuR-microRNA binding controls extracellular export of miR-122 and augments stress response. *EMBO Rep.* **17**, 1184-1203 (2016).

- Aukrust, I. *et al.* The mRNA-binding site of annexin A2 resides in helices C-D of its domain IV. *J Mol Biol* **368**, 1367-1378 (2007).
- McKenzie, A.J. *et al.* KRAS-MEK Signaling Controls Ago2 Sorting into Exosomes. *Cell Rep.* **15**, 978-987 (2016).
- Goldie, B.J. *et al.* Activity-associated miRNA are packaged in Map1b-enriched exosomes released from depolarized neurons. *Nucleic Acids Res.* **42**, 9195-9208 (2014).
- 857 **36.** Melo, S.A. *et al.* Cancer exosomes perform cell-independent microRNA biogenesis and promote tumorigenesis. *Cancer Cell* **26**, 707-721 (2014).
- Liu, J. *et al.* Argonaute2 is the catalytic engine of mammalian RNAi. *Science* **305**, 1437-1441 (2004).
- 861 38. Burroughs, A.M. *et al.* Deep-sequencing of human Argonaute-associated 862 small RNAs provides insight into miRNA sorting and reveals Argonaute 863 association with RNA fragments of diverse origin. *RNA Biol.* **8**, 158-177 864 (2011).
- 39. Czech, B. & Hannon, G.J. Small RNA sorting: matchmaking for Argonautes.

 Nat. Rev. Genet. 12, 19-31 (2011).
- 40. Arroyo, J.D. *et al.* Argonaute2 complexes carry a population of circulating microRNAs independent of vesicles in human plasma. *Proc. Natl. Acad. Sci. U S A* **108**, 5003-5008 (2011).
- Gibbings, D.J., Ciaudo, C., Erhardt, M. & Voinnet, O. Multivesicular bodies associate with components of miRNA effector complexes and modulate miRNA activity. *Nat. Cell Biol.* **11**, 1143-1149 (2009).
- Li, S. *et al.* MicroRNAs inhibit the translation of target mRNAs on the endoplasmic reticulum in Arabidopsis. *Cell* **153**, 562-574 (2013).
- Akers, J.C., Gonda, D., Kim, R., Carter, B.S. & Chen, C.C. Biogenesis of extracellular vesicles (EV): exosomes, microvesicles, retrovirus-like vesicles, and apoptotic bodies. *Journal of neuro-oncology* **113**, 1-11 (2013).
- Wang, J. *et al.* EXPO, an exocyst-positive organelle distinct from multivesicular endosomes and autophagosomes, mediates cytosol to cell wall exocytosis in Arabidopsis and tobacco cells. *Plant Cell* **22**, 4009-4030 (2010).
- Wahlgren, J. *et al.* Plasma exosomes can deliver exogenous short interfering RNA to monocytes and lymphocytes. *Nucleic Acids Res.* **40**, e130 (2012).
- 886 46. Buck, A.H. *et al.* Exosomes secreted by nematode parasites transfer small RNAs to mammalian cells and modulate innate immunity. *Nat. Commun.* **5**, 888 5488 (2014).
- Wu, Z. *et al.* Extracellular vesicle-mediated communication within host-parasite interactions. *Frontiers in immunology* **9**, 3066 (2018).
- 891 48. Boavida, L.C., Qin, P., Broz, M., Becker, J.D. & McCormick, S. Arabidopsis 892 tetraspanins are confined to discrete expression domains and cell types in 893 reproductive tissues and form homo- and heterodimers when expressed

in yeast. Plant Physiol. 163, 696-712 (2013). 894 49. Drakakaki, G. et al. Isolation and proteomic analysis of the SYP61 895 compartment reveal its role in exocytic trafficking in Arabidopsis. Cell Res 896 897 22, 413-424 (2012). 50. Vaucheret, H., Vazquez, F., Crété, P. & Bartel, D.P. The action of 898 ARGONAUTE1 in the miRNA pathway and its regulation by the miRNA 899 pathway are crucial for plant development. *Genes Dev.* **18**, 1187-1197 900

(2004).

901